Geosci. Model Dev., 8, 2749–2776, 2015
www.geosci-model-dev.net/8/2749/2015/
doi:10.5194/gmd-8-2749-2015
© Author(s) 2015. CC Attribution 3.0 License.

Geoscientific Model Development
Open Access

A new chemistry option in WRF-Chem v. 3.4 for the simulation of direct and indirect aerosol effects using VBS: evaluation against IMPACT-EUCAARI data

P. Tuccella[1,2,a], G. Curci[1], G. A. Grell[3,4], G. Visconti[1], S. Crumeyrolle[5,6], A. Schwarzenboeck[5], and A. A. Mensah[7,b]

[1]CETEMPS Centre of Excellence, Dept. Physical and Chemical Sciences, Univ. L'Aquila, L'Aquila, Italy
[2]UPMC Univ. Paris 06, Université Versailles St-Quentin, CNRS/INSU, UMR8190, LATMOS-IPSL, Paris, France
[3]Earth System Research Laboratory, National Oceanic and Atmospheric Administration, Boulder, Colorado, USA
[4]Cooperative Institute for Research in Environmental Sciences, University of Colorado at Boulder, Boulder, Colorado, USA
[5]Laboratoire de Météorologie Physique, Université Blaise Pascal, UMR 6016, Clermont-Ferrand, France
[6]LOA, UMR8518, CNRS – Université Lille1, Villeneuve d'Ascq, France
[7]Institut fur Energie und Klimaforschung: Troposphare (IEK 8), Forschungszentrum Julich GmbH, Julich, Germany
[a]now at: NUMTECH, 6 allée Alan Turing, CS 60242, 63178 Aubiere, France, and Laboratoire de Météorologie Dynamique, Ecole Polytechnique, 91128 Palaiseau, France
[b]now at: Institute for Atmospheric and Climate Science (IAC), ETH Zurich, Zurich, Switzerland

Correspondence to: P. Tuccella (paolo.tuccella@aquila.infn.it)

Received: 8 December 2014 – Published in Geosci. Model Dev. Discuss.: 3 February 2015
Revised: 23 July 2015 – Accepted: 31 July 2015 – Published: 4 September 2015

Abstract. A parameterization for secondary organic aerosol (SOA) production based on the volatility basis set (VBS) approach has been coupled with microphysics and radiative schemes in the Weather Research and Forecasting model with Chemistry (WRF-Chem) model. The new chemistry option called "RACM-MADE-VBS-AQCHEM" was evaluated on a cloud resolving scale against ground-based and aircraft measurements collected during the IMPACT-EUCAARI (Intensive Cloud Aerosol Measurement Campaign – European Integrated project on Aerosol Cloud Climate and Air quality interaction) campaign, and complemented with satellite data from MODIS. The day-to-day variability and the diurnal cycle of ozone (O_3) and nitrogen oxides (NO_x) at the surface are captured by the model. Surface aerosol mass concentrations of sulfate (SO_4), nitrate (NO_3), ammonium (NH_4), and organic matter (OM) are simulated with correlations larger than 0.55. WRF-Chem captures the vertical profile of the aerosol mass concentration in both the planetary boundary layer (PBL) and free troposphere (FT) as a function of the synoptic condition, but the model does not capture the full range of the measured concentrations. Predicted OM concentration is at the lower end of the observed mass concentrations. The bias may be attributable to the missing aqueous chemistry processes of organic compounds and to uncertainties in meteorological fields. A key role could be played by assumptions on the VBS approach such as the SOA formation pathways, oxidation rate, and dry deposition velocity of organic condensable vapours. Another source of error in simulating SOA is the uncertainties in the anthropogenic emissions of primary organic carbon. Aerosol particle number concentration (condensation nuclei, CN) is overestimated by a factor of 1.4 and 1.7 within the PBL and FT, respectively. Model bias is most likely attributable to the uncertainties of primary particle emissions (mostly in the PBL) and to the nucleation rate. Simulated cloud condensation nuclei (CCN) are also overestimated, but the bias is more contained with respect to that of CN. The CCN efficiency, which is a characterization of the ability of aerosol particles to nucleate cloud droplets, is underestimated by a factor of 1.5 and 3.8 in the PBL and FT, respectively. The comparison with MODIS data shows that the model overestimates the aerosol optical thickness (AOT). The domain averages (for 1 day) are 0.38 ± 0.12 and 0.42 ± 0.10 for MODIS and WRF-Chem data, respectively. The droplet effective radius (R_e) in liquid-phase clouds is underestimated by a factor of 1.5; the cloud liquid water path (LWP) is overestimated by a factor of 1.1–

1.6. The consequence is the overestimation of average liquid cloud optical thickness (COT) from a few percent up to 42 %. The predicted cloud water path (CWP) in all phases displays a bias in the range +41–80 %, whereas the bias of COT is about 15 %. In sensitivity tests where we excluded SOA, the skills of the model in reproducing the observed patterns and average values of the microphysical and optical properties of liquid and all phase clouds decreases. Moreover, the run without SOA (NOSOA) shows convective clouds with an enhanced content of liquid and frozen hydrometers, and stronger updrafts and downdrafts. Considering that the previous version of WRF-Chem coupled with a modal aerosol module predicted very low SOA content (secondary organic aerosol model (SORGAM) mechanism) the new proposed option may lead to a better characterization of aerosol–cloud feedbacks.

1 Introduction

It is well recognized that aerosol particles have a fundamental role in the climate system. They directly alter the budget of the radiation that reaches the Earth's surface by scattering and absorbing the incoming sunlight (Haywood and Boucher, 2000), and they indirectly affect cloud properties and precipitation patterns, because they act as cloud condensation nuclei (CCN) (Rosenfeld et al., 2008; Lohmann and Feichter, 2005). Some aerosol species as black and brown carbon or mineral dust heat the atmosphere absorbing the solar radiation. The local warming may increase the atmospheric stability, leading to a decrease in cloud cover through the so-called semi-direct effect (Hansen et al., 1997). The global mean radiative forcing associated with aerosols, as a result of changes in anthropogenic emissions since pre-industrial times, is highly uncertain and is estimated to be $-0.9\,\mathrm{W\,m^{-2}}$, with an uncertainty range of -1.9 to $-0.1\,\mathrm{W\,m^{-2}}$ (Boucher et al., 2013).

Experimental evidence of the influence of aerosols on cloud macrophysical and microphysical properties has been shown in several works (Clarke and Kapustin, 2010; Christensen and Stephen, 2011; Koren et al., 2012; Ten Hoeve et al., 2011; Li et al., 2011). Several modelling studies show that aerosol particles have a strong impact not only on the climatic spatial–temporal scale but also at short range on the regional scale (Baklanov et al., 2014). At regional scale, online coupled mesoscale meteorology–chemistry models are useful tools to take into account aerosol feedback effects on both meteorology and atmospheric composition (Zhang, 2008; Baklanov et al., 2014).Weather Research and Forecasting model with Chemistry model (WRF-Chem), which is the model used in this study, is one of such models (Grell et al., 2005; Fast et al., 2006; Chapman et al., 2009). In this work we present and evaluate some developments of WRF-Chem for a better simulation of direct and indirect aerosol feedback.

The introduction of the aerosol–cloud–radiation feedback leads to non-linear chains and loops of interactions between meteorological and chemical processes that are inhomogeneous in space and time (Baklanov et al., 2014). Furthermore, the prediction of meteorological variables significantly improves when the direct and indirect aerosol effects are taken into account in numerical simulation. For example, Yang et al. (2011) found that the inclusion of aerosol feedback produces significant benefits in the simulated optical and microphysical properties of marine stratocumulus, and these improvements positively affect the simulation of the boundary layer structure and energy budget. Yu et al. (2014) reported an improvement of the simulation of shortwave and long-wave cloud forcing when the aerosol feedback is added to the model.

Recent studies conducted with global models, predict an important contribution of secondary organic aerosol (SOA) to direct and indirect aerosol feedback. O'Donnell et al. (2011) calculated an annual mean direct and indirect shortwave forcing of -0.31 and $+0.23\,\mathrm{W\,m^{-2}}$, respectively. Biogenic SOA (BSOA) seems to play an important role on aerosol–cloud–radiation interaction. Scott et al. (2014) find that BSOA contributes 4–21 % to the global annual mean of CCN and 2–5 % to global mean of cloud droplet concentration. They also attribute BSOA to a global mean indirect radiative forcing that ranges from -0.77 to $+0.01\,\mathrm{W\,m^{-2}}$.

Previous studies over USA and Europe demonstrated that the "traditional" configuration of WRF-Chem (Grell et al., 2005), using the secondary organic aerosol model (SORGAM) (Schell et al., 2001), presents a negative bias of simulated $PM_{2.5}$ mass, mostly attributable to a scarce production of SOA (Grell at al., 2005; McKeen et al., 2007; Tuccella et al., 2012). Therefore, an updated "chemistry option" with a more sophisticated treatment of SOA, fully coupled with radiative and microphysics modules, is highly desirable. In Sect. 2 of this work, we describe the developments of WRF-Chem code carried out in order to simulate the direct and indirect effects with the new SOA parameterization (based on the volatility basis set, VBS, approach) recently implemented in the model by Ahmadov et al. (2012). In Sect. 3, we describe the measurements used to evaluate the model. In Sect. 4, we evaluate the performance of the updated model through a comparison with satellite data and with meteorological and chemical constituent measurements performed in the frame of the European Integrated project on Aerosol Cloud Climate and Air quality interaction (EUCAARI) (Kulmala et al., 2011). The aim of the Sect. 5 is to address the two following questions: (1) does the introduction of SOA particles interacting with radiation and cloud processes improve the numerical prediction of cloud fields? (2) What is the potential impact of SOA particles on cloud development? The final remarks are given in Sect. 6.

2 WRF-Chem model

2.1 Description and upgrade

A pre-release of version 3.4 of the WRF-Chem (Grell et al., 2005) was used in this study. WRF-Chem is a community model that has many options for gas chemistry and aerosols. One of these has been updated in order to include a new chemistry option for simulation of direct and indirect effects with an updated parameterization for SOA production. The modifications introduced by Fast et al. (2006), Chapman et al. (2009), and Ahmadov et al. (2012) are the basis of our work. The technical details of the implementation are summarized in Appendix A.

The gas-phase mechanism used is an updated version of the regional atmospheric chemistry mechanism (RACM) (Stockwell et al., 1997). The inorganic aerosols are treated with the Modal Aerosol Dynamics Model for Europe (MADE) (Ackermann et al., 1998). The updated parameterization for SOA production is based on the VBS approach (Ahmadov et al., 2012). MADE-VBS model has three log-normal modes: Aitken, accumulation and coarse. The species treated are the sulfate ($SO_4^=$), nitrate (NO_3^+), ammonium (NH_4^+), elemental carbon (EC), primary organic matter (POM), SOA (anthropogenic and biogenic), chloride (Cl), sodium (Na), unspeciated $PM_{2.5}$ (that includes the fine fraction of sea salt and soil dust), aerosol water, unspeciated coarse fraction of PM_{10}, soil dust, and sea salt.

SOA parameterization implemented by Ahmadov et al. (2012) is based on a four bin volatility basis set, with a saturation concentration of 1, 10, 100, and 1000 $\mu g\,m^{-3}$ at 300 K. Volatile organic compounds (VOCs) are oxidized by reactions with hydroxyl radical (OH), ozone (O_3), and nitrate radical (NO_3). Oxidized VOCs are anthropogenic (alkanes, alkenes, toluene, xylene, and cresol) and biogenic (isoprene, monoterpenes, and sesquiterpenes). In each bin, organic mass is produced for two different regimes, high and low NO_x. In the former, organic peroxy radicals react with nitrogen oxide (NO); conversely, in the latter organic peroxy radicals react with other organic peroxy radicals. The organic matter produced is partitioned into aerosol and gas phase assuming a pseudo-ideal partition. Organic condensation vapours (OCVs) produced by the oxidation of VOCs may be oxidized by reacting with OH, consequently reducing the vapour pressure and shifting mass from high-volatility bins to lower ones. The default oxidation rate (or ageing factor) used in the model is $1.0 \times 10^{-11}\,cm^3\,molec.^{-1}\,s^{-1}$ for both anthropogenic and biogenic OCVs. The ageing factor is one the key uncertainties in SOA formation in the VBS approach. The other two important factors of uncertainty are those related to the SOA formation pathways and to the dry deposition velocity of OCVs. The latter is assumed to be 25 % of the dry deposition velocity of nitric acid (HNO_3).

The implementation of aerosol–cloud–radiation interaction within RACM-MADE-VBS follows the methods described by Fast et al. (2006) and Chapman et al. (2009). We modified the WRF-Chem code by preparing the inputs for the modules devoted to calculation of the aerosol optical properties and the aerosol activation, starting from the mass of each aerosol type as predicted by the new chemistry package. In the approach of Fast et al. (2006), the three modes of the log-normal distribution are divided into eight bins, and each chemical constituent of the aerosol mass is associated with a complex refractive index. The refractive index is calculated for each bin with a volume average. Mie theory is used to find the scattering and absorption efficiencies. Aerosol optical thickness (AOT), single scattering albedo, and asymmetry parameter calculated with the optical package developed by Barnard et al. (2010) are used as input to the radiative scheme (Goddard and RRTMG). The aerosol direct effect on long-wave radiation is included following Zhao et al. (2010).

Aerosol–clouds interaction is a complex problem that involves the activation and resuspension of the aerosol particles, aqueous chemistry, and wet removal. Following Chapman et al. (2009), aerosols within cloud droplets are treated as "cloud borne". Aerosols that do not activate as cloud droplets are treated as "interstitial". In WRF-Chem the activation process is based on the parameterization developed by Abdul-Razzak and Ghan (2000, 2002). The number and mass concentration of the activated aerosols are calculated for each mode. The activation of aerosols is based on a maximum supersaturation determined from a Gaussian spectrum of updraft velocities and bulk hygroscopicity of each aerosol compound for all log-normal modes of particles. Bulk hygroscopicity is based on the volume-weighted average of the hygroscopicity of each aerosol component. In addition to the activated aerosols at environmental conditions, the CCN spectrum is also determined; i.e. the aerosol particles acting as CCN at some given maximum supersaturations (0.02, 0.05, 0.1, 0.2, 0.5, and 1 %) are calculated.

Within the dissipating clouds, the droplets evaporate and the cloud borne aerosols are resuspended to the interstitial state. Cloud borne aerosols and dissolved trace gases may be modified by aqueous chemistry. In this chemistry option, cloud chemistry is modelled using the scheme of Walcek and Taylor (1986). Wet deposition of trace gases and aerosols is treated in and below clouds. Within clouds the aerosols and trace gases dissolved in the water are collected by rain, graupel, and snow. Below clouds the wet scavenging by precipitation is parameterized using the approach of Easter et al. (2004).

The simulation of the activation, resuspension, and wet scavenging of the aerosol particles requires a prognostic treatment of the cloud droplets. The prognostic treatment of the cloud droplets takes into account the losses due to collision, coalescence, collection, and evaporation, and the source due to nucleation. The Lin and Morrison microphysics schemes in WRF-Chem version 3.4 include the prognostic treatment of the cloud droplet number concentration. The source due to nucleation is parameterized following

Table 1. Physical and chemical parameterizations used in the simulation.

Physical processes	WRF-Chem parameterizations
Cloud microphysics	Morrison
Cumulus cloud	New Grell (D1 and D2)
Long-wave radiation	RRTM
Shortwave radiation	RRTM
PBL	MYNN
Surface layer	Monin-Obukhov
Surface	Noah Land Surface Model
Gas-phase chemistry	Modified RACM-ESRL
Aerosol chemistry	MADE/SOA-VBS
Biogenic emissions	MEGAN

Ghan et al. (1997). Both microphysical schemes take into account the autoconversion of cloud droplets to rain dependent on the cloud droplet number. Therefore, aerosol activation affects both the rain rate and the liquid water content. The droplet number concentration affects the calculation of the cloud droplet effective radius and cloud optical thickness (COT). The interaction of clouds with the incoming shortwave radiation is done by linking the microphysics to the radiation scheme. The reader should note that the contribution to SOA concentration by cloud chemistry is missing and the interaction of aerosol with ice nuclei is not taken into account in this version of the model.

2.2 Model configuration

The simulations were conducted over three one-way nested domains centred on the Netherlands, as shown in Fig. 1. The coarse domain (D1) has 30 km horizontal resolution, domain 2 (D2) 10 km, and domain 3 (D3) is cloud resolving at 2 km resolution. In our runs we used 67 vertical levels extending up to 50 hPa.

The main physical and chemical parameterizations used are listed in Table 1. The model setup is the same for all three domains, except that no cumulus parameterization is used for D3. Wet scavenging and cloud chemistry from both parameterized updraft and resolved clouds are taken into account in D1 and D2. However, in these domains the sub-grid cloud processes involve only the interstitial aerosol, i.e. the aerosol–cloud coupling is not considered in convective parameterization. Therefore, the indirect effects are well resolved for domains with resolution less than 10 km in the version of WRF-Chem used in this work.

As mentioned in Sect. 2.1, two key uncertainties in SOA production are the deposition velocity and ageing factor of OCVs. The first is assumed to be 25 % (this value is called "deposition factor" in WRF-Chem) of dry deposition velocity of HNO_3; the second is set to 1.0×10^{-11} cm^3 molec.$^{-1}$ s^{-1}. Ahmadov et al. (2012) showed that by reducing the ageing factor of OCVs by 50 %, daily average concentration of SOA decreases by 20 %, and an increase of the dry deposition velocity of OCVs by a factor of 4 brings about an SOA concentration decreases by 50 %. Deposition factor and ageing are tunable parameters. After some sensitivity tests, we chose the default value for deposition factor and 5.0×10^{-11} cm^3 molec.$^{-1}$ s^{-1} as ageing of OCVs, because this combination minimizes the model bias with observations.

We simulated the period from 14 to 30 May 2008. We chose this period because aerosol and cloud state-of-art measurements were available to evaluate the model (see Sect. 3). Moreover, during this period anticyclonic and cyclonic meteorological conditions were observed which allows for the evaluation of the model under varying conditions. The initial and boundary meteorological conditions for D1 are provided by the European Centre for Medium range Weather Forecast (ECMWF) analyses with a horizontal resolution of 0.5° every 6 h. The chemical boundary conditions of D1 are taken from output of the global Model for Ozone and Related Chemical Tracers (MOZART) (Emmons et al., 2010). MOZART output has been converted to RACM/MADE/SOA-VBS species by using the "mozbc" interface that may be downloaded from the http://ruc.noaa.gov/wrf/WG11/.

A series of 30 h simulations were performed on each day starting at 00:00 UTC, with the first 6 h discarded as model spin-up for meteorology. Meteorology of D1 is reinitialized from global analysis, while initial and boundary meteorology conditions for D2 and D3 are taken from D1 and D2, respectively. For all three domains, the chemical initial state is restarted from the previous run, while the chemical boundary conditions of D2 and D3 are taken from D1 and D2, respectively. The first 13 days of May 2008 are also simulated to spin-up the chemistry.

2.3 Emissions

Anthropogenic emissions data are taken from the Netherlands Organization for Applied Scientific Research (TNO) 2007 inventory (Kuenen et al., 2014). TNO is a gridded European inventory with resolution of $0.125° \times 0.0625°$. It provides the anthropogenic emissions of NO_x, non-methane volatile organic compounds (NMVOCs), NH_3, sulfur dioxide (SO_2), CO, primary $PM_{2.5}$, and PM_{10}. EC and primary OC emissions are taken from a specific TNO database that is part of the EUCAARI project (Kulmala et al., 2011). These EC and OC emissions are size resolved, they are separated for particles less than 1 µm, particles in the range of 1–2.5 and 2.5–10 µm.

Horizontal and vertical interpolation, temporal disaggregation, NMVOC speciation, and aggregation of emissions into WRF-Chem species is done following Tuccella et al. (2012), with minor updates described in Curci et al. (2015a). In order to prevent spurious concentration of aerosol particles, the distribution of aerosol emissions into

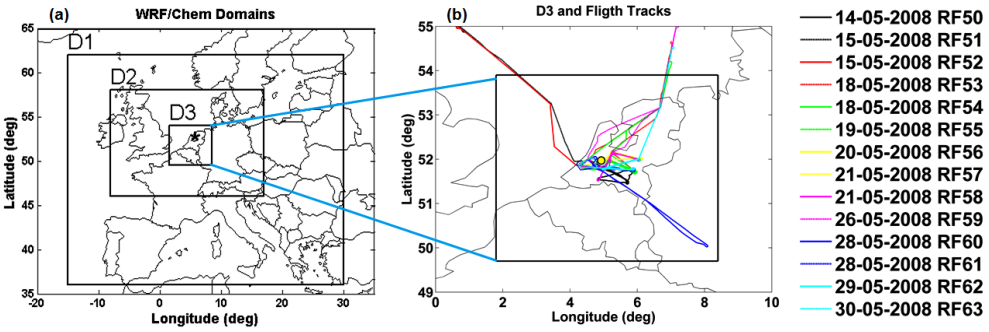

Figure 1. Panel **(a)** shows the three nested model domains used for simulations. D1 is 30 km resolution, D2 10 km, and D3 2 km. The black star indicates the Cabauw supersite. Panel **(b)** is a zoom of D3 and shows the track of every flights used in this study, yellow circle represents Cabauw supersite.

WRF-Chem modes is based on the low emission scenario of Elleman and Covert (2010). In all 10 % of the emitted aerosol mass is attributed to Aitken mode, and 90 % to the accumulation mode.

Biogenic emissions are calculated online with Model of Emissions of Gases and Aerosols from Nature (MEGAN) (Guenther et al., 2006). Dust and sea salt emissions from soil and seawater are calculated online in the simulations.

3 Measurements

We evaluated model performances in D3 against ground and aircraft-based data collected in May 2008 during the Intensive Cloud Aerosol Measurement Campaign (IMPACT) in the frame of the EUCAARI project (Kulmala et al., 2011). Model results were also evaluated against MODIS satellite data.

An overview of the synoptic conditions of May 2008 over central Europe is given by Hamburger et al. (2011). The first 15 days of May are characterized by an anticyclonic block, while the period from 16 to 31 is dominated by westerly wind and passage of several fronts. The days from 17 to 20 May are referred as "scavenged background situation" (Mensah et al., 2012), because they are dominated by a northerly wind from the North Sea associated with a low aerosol mass loading, due to wet scavenging. The period starting from 23 May is dominated by long-range transport of dust from Sahara desert (Roelofs et al., 2010; Bègue et al., 2015).

3.1 Ground-based measurements

Meteorological and aerosol ground-based measurements used in this study are collected in Cabauw (the Netherlands) at Cabauw Experimental Site for Atmospheric Research (CESAR) observatory Cabauw (Fig. 1). CESAR observatory is a tower located at 51°57′ N, 4°54′ E, and −0.7 m a.s.l., at about 50 km south of Amsterdam. Measurements performed at CESAR observatory are typical of north-west Europe, and are representative of maritime and continental conditions depending on the wind direction (Mensah et al., 2012).

Standard meteorological variables are collected at 2, 10, 20, 40, 80, 140, and 200 m height. Furthermore, in this study we used the measurements of temperature and relative humidity profiles obtained with radiometer, and aerosol speciation from aerosol mass spectrometry (AMS) collected at 60 m (Mensah et al., 2012).

The model is also compared to O_3, nitrogen oxide (NO_x), nitric dioxide (NO_2), NO, ammonia (NH_3), HNO_3, nitrous acid (HONO), and SO_2 measurements issued by Cabauw Zijdeweg EMEP (European Monitoring and Evaluation Programme) station (NL0011R). O_3 is measured with an ultraviolet absorbing ozone instrument, NO_x, NO. and NO_2 with a chemiluminescence monitor, and NH_3, HNO_3, HONO, and SO_2 with an online ion chromatograph.

Although Cabauw supersite provides very detailed measurements, it could not be enough to characterize the model performance near the surface. Therefore, WRF-Chem is also compared to daily PM_{10} data from 63 stations (10 rural, 25 suburban, and 28 urban) of AIRBASE network and to daily inorganic aerosol measurements issued at Bilthoven (NL0008R), Kollumerward (NL0009R), Vredepeel (NL00010R), and De Zilk (NL00091R) EMEP stations. SO_4 and NH_4 measurements are also performed at all these sites, while NO_3 measurements are available only at De Zilk.

3.2 Aircraft measurements

During May 2008, a French ATR-42 research aircraft performed 22 research flights (RF). In this work we used 14 RF to evaluate the model. Their tracks are reported in Fig. 1, while flight number and take-off and landing time are reported in Table S1 in the Supplement. RF50, RF55, RF56, RF57, RF58, RF61, and RF62 were conducted around the Cabauw supersite, in order to study the origin and characteristic of air masses collected at Cabauw. Other RFs were aimed at the study of aerosol properties along a quasi-Lagrangian flight track, with west–east and north–south tran-

sects. ATR-42 was equipped with instrumentation suitable for aerosol–cloud interaction measurements. We used the measurements from a condensation particle counter (CPC), the CPC3010 with a cut-off size of 15 nm, a Cloud Condensation Nuclei Counter (CCNC) for CCN number concentration measurements, and an AMS. During the campaign a scanning mobility particle sizer (SMPS) was used to measure the number size distribution of aerosol particles with a diameter in the range of 0.02–0.5 µm, while the size distribution of aerosol particles larger than 100 nm was sampled with a passive cavity aerosol spectrometer probe (PCASP). SMPS and PCASP measurements were combined in order to calculate the $PM_{2.5}$ concentration using an average aerosol density of 1.7 g m^{-3}. A more exhaustive and detailed description of the whole campaign and instrumentation is given by Crumeyrolle et al. (2013).

3.3 Satellite measurements

The model was also evaluated with MODIS-Aqua aerosol and cloud data. The Level 2 products used here are MYD04 and MYD06 collection 051 for aerosol and clouds, respectively. For ease of comparison with model output, both satellite and model data were regridded onto a common lat.–long. regular grid. Model output is sampled at same time and location of each MODIS pixel, and then data are averaged in space and time over the same grid. In this study the horizontal spacing of the common grid is 4 km.

4 Model evaluation

Model results are compared to ground-based and aircraft observations, as detailed in Sect. 3. The statistical indices used are the Pearson's correlation coefficient (r), mean bias (MB), normalized mean bias (NMB), and normalized mean gross error (NMGE). The indices are defined in the Appendix and reported in Table 2.

4.1 Meteorology

Figure 2 shows the observed and modelled time series of hourly vertical profiles of temperature and relative humidity at the Cabauw supersite. WRF-Chem reproduces the day-to-day variation of temperature, before, after, and during the wet period. As shown by statistical indices (Table 2), within the first 200 m, the model reproduces the temperature with a correlation of 0.93–0.95 and a mean bias of about −0.5 °C. Looking at the free troposphere, we may realize that the model underestimates the height of the 0° C isotherm (the black line on Fig. 2a) in the first days of simulation and during the wet period by about 200–300 m (i.e., the model is colder than observed by 1–1.5 °C). Whereas immediately after the passage of the cold front, the temperature rise in the simulation is slower than the observed one. The model performances in simulating surface temperature are consistent with other European studies (e.g., Zhang et al., 2013a; Brunner et al., 2015). For example, Brunner et al. (2015) compared several meteorology–chemistry coupled models with annual simulations at continental scale, and found that on central Europe the predicted surface temperature shows a correlation with observations in the range of 0.95–0.98, whereas the bias ranges from −1 to 0.1 °C.

Table 2. Statistical indices of the comparison of WRF-Chem to observations of temperature (T), relative humidity (RH), wind speed (WS), wind direction (WD), ozone (O_3), nitrogen oxide (NO_x), nitric dioxide (NO_2), nitric oxide (NO), ammonia (NH_3), nitric acid (HNO_3), nitrous acid (HONO), sulfur dioxide (SO_2), particle sulfate (SO_4), particle nitrate (NO_3), particle (ammonium), and particle OM, collected at Cabauw tower.

Variable	R	MB	NMB	NMGE
T (°C) at 2 m	0.93	−0.66	−5.46	10.65
T (°C) at 10 m	0.93	−0.67	−5.24	9.31
T (°C) at 20 m	0.94	−0.56	−4.15	8.16
T (°C) at 40 m	0.94	−0.46	−3.24	7.21
T (°C) at 80 m	0.95	−0.32	−2.10	5.97
T (°C) at 140 m	0.95	−0.26	−1.51	5.92
T (°C) at 200 m	0.95	−0.45	−2.79	6.66
RH (%) at 2 m	0.87	3.17	6.42	11.23
RH (%) at 10 m	0.89	4.44	8.36	11.48
RH (%) at 20 m	0.91	3.04	6.33	10.50
RH (%) at 40 m	0.92	2.99	6.40	10.51
RH (%) at 80 m	0.73	−1.04	2.13	13.34
RH (%) at 140 m	0.92	2.81	6.40	11.19
RH (%) at 200 m	0.91	2.99	7.44	12.50
WS (m s^{-1}) at 10 m	0.78	0.67	27.90	35.56
WS (m s^{-1}) at 20 m	0.66	1.27	40.89	49.32
WS (m s^{-1}) at 40 m	0.67	1.26	32.64	42.04
WS (m s^{-1}) at 60 m	0.72	1.23	24.42	38.99
WS (m s^{-1}) at 140 m	0.74	1.21	28.66	41.55
WS (m s^{-1}) at 200 m	0.76	1.13	27.79	41.48
WD (°) at 10 m	0.52	27.32	43.31	43.31
WD (°) at 20 m	0.53	24.80	40.48	40.48
WD (°) at 40 m	0.60	23.59	40.34	40.34
WD (°) at 80 m	0.67	20.22	30.34	30.34
WD (°) at 140 m	0.71	19.21	32.01	32.01
WS (°) at 200 m	0.73	17.18	28.46	28.46
O_3 (µg m^{-3})	0.72	−3.43	70.03	90.88
NO_x (µg m^{-3})	0.70	0.43	19.76	44.77
NO (µg m^{-3})	0.65	0.28	116.08	167.59
NO_2 (µg m^{-3})	0.66	1.25	28.68	54.20
NH_3 (µg m^{-3})	0.43	−4.75	−27.72	42.94
HNO_3 (µg m^{-3})	0.21	−0.09	−1.22	108.65
HONO (µg m^{-3})	0.05	−0.56	−95.37	95.37
SO_2 (µg m^{-3})	0.48	0.68	90.20	116.33
SO_4 (µg m^{-3})	0.56	1.04	92.2	95.4
NO_3 (µg m^{-3})	0.68	1.00	72.4	94.3
NH_4 (µg m^{-3})	0.74	0.66	63.0	67.3
OM (µg m^{-3})	0.75	−0.42	3.21	29.9

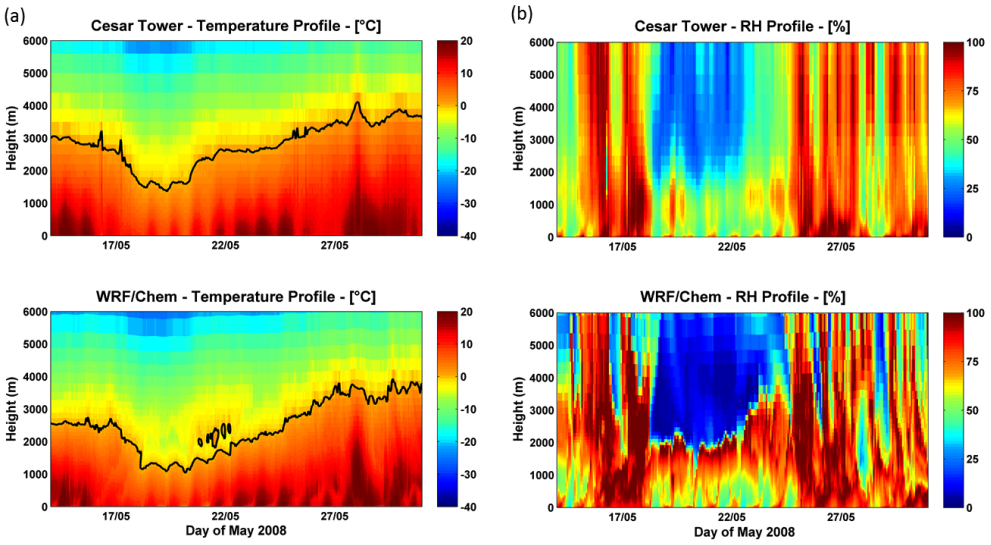

Figure 2. Observed and simulated time series of vertical profile of the temperature **(a)** and relative humidity **(b)**, observed at Cesar observatory. The black line on the temperature profile represents the 0 °C isotherm.

The model reproduces the vertical structure of relative humidity (Fig. 2b) over the whole period, but it has the tendency to overestimate (underestimate) the higher (lower) observed values. This behaviour is more evident during scavenging days, when the relative humidity between 1000 and 2000 m is overestimated on average by 40 %, but sometimes up to 60 %. Errors of this magnitude in simulating the vertical profile of RH were already found in previous works (Misenis and Zhang, 2011; Luo and Yu, 2011). Nevertheless, the model correlation and mean bias are 0.84 and +3.4 % below 1000 m of altitude, 0.50 and +13 % in the range of 1000–2000 m, and 0.78 and +6.4 % between 2000 and 3000 m. These values are comparable with those found by Fast et al. (2014) in the comparison of WRF-Chem simulations to aircraft data. They have shown correlations in the interval of 0.49–0.70, while the bias is from −7 to +0.1 %. Near the surface, the relative humidity is simulated with a correlation of 0.87–0.92 and a positive MB of 3–4 % (+6–8 %).

The biases of the temperature and relative humidity could be due to a misrepresentation of soil (and sea) temperature and soil moisture or by misrepresentation of the clouds and rain. These two problems are tightly coupled via land surface–atmosphere interaction. The errors in the simulation of surface moisture and energy budget influences the fluxes of latent heat and moisture in the atmosphere, affecting the local circulation, convective available potential energy (CAPE), cloud formation, and rain pattern (Pielke, 2001; Holt et al., 2006). Moreover, WRF-Chem tends to fail simulating the thermodynamic variables near coastlines, because the uncertainties of land use data may play an important role (Misenis and Zhang, 2010). Initial and boundary meteorological conditions may also play an important role. Bao et al. (2005) demonstrated that meteorological prediction is sensitive to used input data. They showed that varying the inputs used as initial and boundary conditions, the mean daily model bias ranges from −2.71 to −0.65 K for the temperature and from −0.81 to 0.50 g kg^{-1} for vapour water content.

In Fig. 3 we compare the time series of observed and predicted wind speed and direction at several heights of Cabauw tower. WRF-Chem captures the diurnal trend of wind speed, but it overestimates the wind speed during the night. Generally, we found the higher correlation at 10 and 200 m (0.78 and 0.76 respectively) and higher NMB between 20 and 40 m (+30–40 %). The wind direction is captured at all altitude levels of Cabauw tower, except on 18 May when WRF-Chem does not reproduce some rapid variations most likely due to local effects. The simulation of wind direction tends to improve with height. Indeed, the correlation coefficient increases from 0.52 to 0.73 at 10 and 200 m, respectively, and the MB decreases from 27° below 40 m to 17° at 200 m. The performance in simulating the surface wind speed are consistent with those reported by Brunner et al. (2015) in central Europe. They have shown a correlation for 10 m wind speed in the range of 0.53–0.73 and a mean bias of 1–1.8 m s^{-1}. It is well recognized that WRF tends to overestimate the wind near the surface (e.g. Misenis and Zhang, 2010; Ngan et al., 2013; Brunner et al., 2015), but the bias of the simulated wind speed could be also explained with uncertainties in the large-scale pattern of analysis used as input. Bao et al. (2005) showed that varying the meteorological inputs, the mean daily model bias may range from −1.53 to −0.28 and from −1.43 to 0.01 m s^{-1} for the u and v component of the wind, respectively.

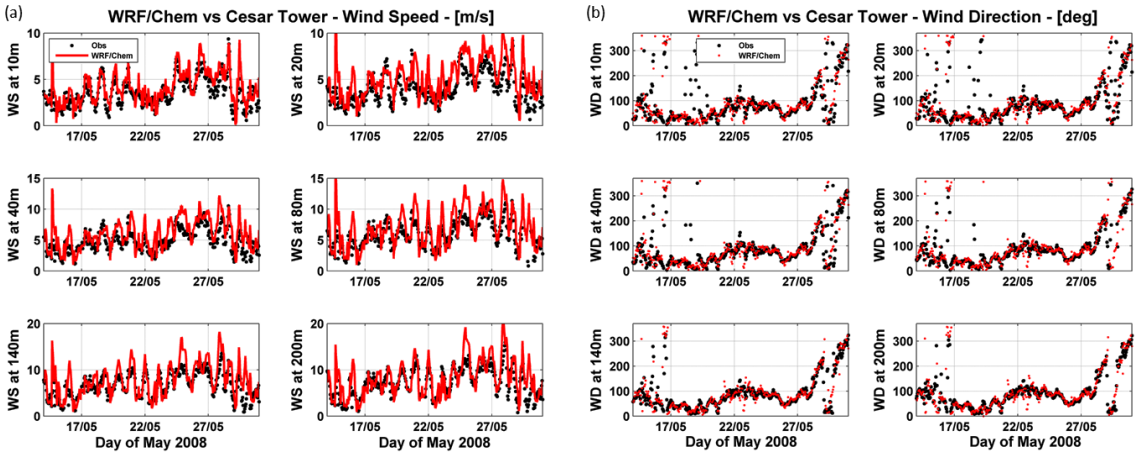

Figure 3. Observed (black lines) at Cesar tower and simulated (red lines) time series of wind speed **(a)** and wind direction **(b)** at different heights.

4.2 Surface gas phase and aerosol mass

Figure 4 displays the comparison between the observed and modelled hourly time series and average diurnal cycles of O_3, NO_x, NO_2, NO, NH_3, HNO_3, HONO, and SO_2 near the surface.

WRF-Chem reproduces the day to day variations of O_3, capturing its decrease during scavenging period due to low photolysis rate caused by cloud presence, recovery in the following days, and a new decrease starting from 25 May. The average daily cycle is well reproduced with a morning minimum and an underestimated maximum in the afternoon. The model simulates the O_3 with a correlation of 0.72 and systematic negative bias on average about 3.4 $\mu g\,m^{-3}$. This bias is observed in the afternoon and the evening, and is most likely due to the titration in these hours caused by higher NO_x concentration than observed.

WRF-Chem simulates the NO_x, NO, and NO_2 time series with a correlation of 0.70, 0.65, and 0.66, respectively. The timing of NO_x daily cycle is reproduced. Indeed, the model captures the morning and evening peaks as well as the diurnal minimum of NO_2. The mean bias of modelled NO_2 is $+1.25\,\mu g\,m^{-3}$ (+20 %) and occurs in the afternoon and evening hours. Moreover, WRF-Chem reproduces the morning peak and diurnal decrease of NO, but the daily cycle is affected by an average positive bias of $0.28\,\mu g\,m^{-3}$, with the average morning maximum overestimation of about $2\,\mu g\,m^{-3}$ (+33 %).

Ammonia is reproduced with a correlation of 0.43. WRF-Chem underestimates the NH_3 during the scavenging days and from 28 to 31 May. The model captures the daily cycle shape of NH_3 concentration average, but the modelled NH_3 concentrations are constantly underestimated. The negative mean bias over the whole period is on average about $-4.75\,\mu g\,m^{-3}$ (−28 %). WRF-Chem reproduces the observed HNO_3 with a poor correlation. The measured mean diurnal cycle is flat; conversely, the model predicts a nocturnal minimum and diurnal maximum. The origin of model bias in simulating NH_3 and HNO_3 is discussed below, together with a discussion on inorganic aerosols.

The nitrous acid concentrations are not well captured by the model and are underestimated by 95 %. This bias could be partly explained by the inefficiency of NO oxidation, the only important reaction known to form HONO. Li et al. (2014), indeed, demonstrated that the major sources of HONO are some unknown reactions that consume nitrogen oxides and hydrogen oxide radicals.

The model reproduces the measured SO_2 with a correlation of 0.48 and a positive bias of $0.68\,\mu g\,m^{-3}$ (+90 %). The overprediction is most likely attributable to anthropogenic emissions. SO_2 is emitted mainly from isolated and elevated large-point sources (Fig. S1 in the Supplement) that are immediately mixed in the model cell leading to overestimation outside of the local plume (Stern et al., 2008). This is demonstrated, for example, by the larger NMGE for SO_2 than NO_x (116 and 45 %, respectively). NO_x is emitted near the surface by traffic and domestic heating. Therefore, NO_x emissions are subjected to a stronger temporal modulation than SO_2 point sources.

The different uncertainties found for the involved species may depend on the choice of the chemical mechanism. Knote et al. (2015a) compared several chemical mechanisms within a box model constrained by the same meteorological conditions and emissions, and found that the prediction of the O_3 diurnal cycle differs by less than 5 % among the different mechanisms. Larger differences were found for other species. For example, the key radicals exhibit differences up to 40 % for OH, 25 % for H_2O_2, and 100 % for NO_3 among the selected mechanisms.

Figure 5 shows the simulated and observed time series and diurnal cycle of aerosol sulfate, nitrate, ammonium, and organic matter, at CESAR observatory. WRF-Chem simulates

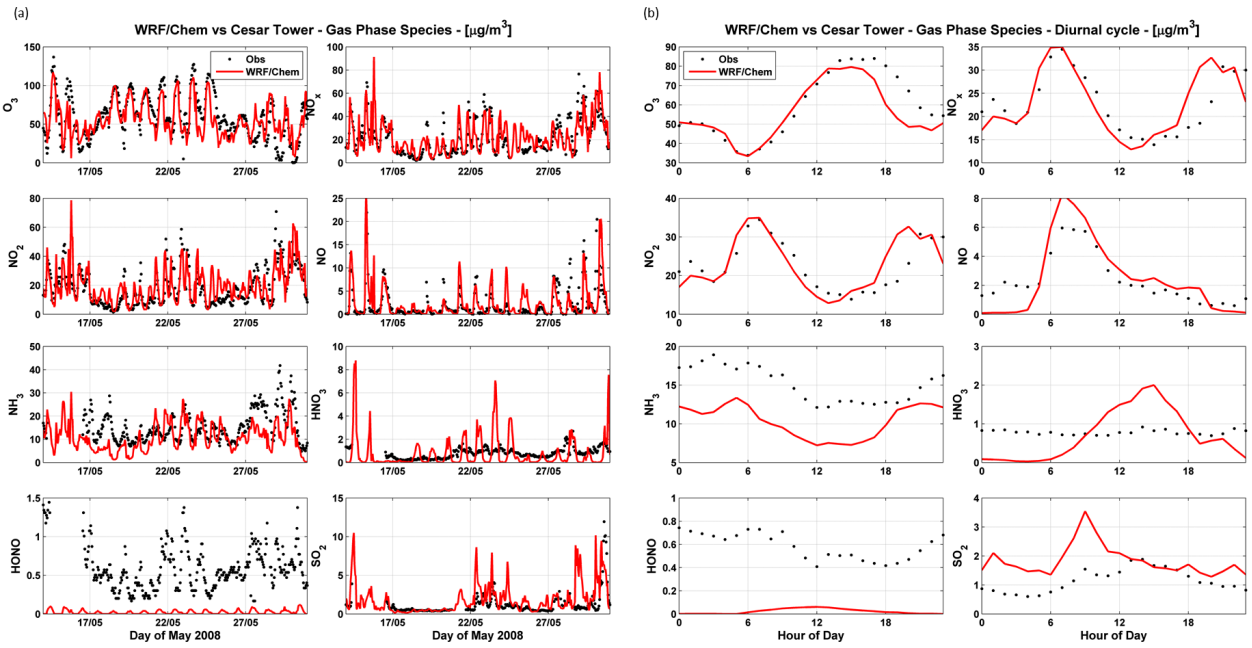

Figure 4. Observed and simulated time series of gas-phase species **(a)** and their average diurnal cycle **(b)**, at Cabauw Zijdeweg EMEP station (NL0011R).

the measured SO_4, NO_3, and NH_4 with a correlation of 0.56, 0.68, and 0.66, respectively.

WRF-Chem captures the daily variations of SO_4 and its decrease during scavenging days. The shape of the diurnal cycle is also reproduced, with the night-time minimum and diurnal maximum. The mass concentration of SO_4 is overpredicted for the whole period with a mean bias of 1.04 $\mu g\,m^{-3}$ (+90 %). The modelled SO_4 overestimation is directly attributable to SO_2 concentration overprediction. Another potential source of the surplus of simulated SO_4 is related to an excessive production within the clouds. Indeed, during scavenging days, the particulate sulfate is overestimated, while the predicted SO_2 does not show a bias in respect to the measurements. The overestimation of SO_4, moreover, explains in part the negative bias of predicted NH_3. The excess of particle sulfate consumes too much ammonia (Meng et al., 1997).

NO_3 is reproduced with a positive bias of 1 $\mu g\,m^{-3}$ (+72 %). Looking at diurnal cycle, the modelled nitrate is on average biased high in the daytime, with a peak in the afternoon. This maximum appears to be correlated with HNO_3 maximum. Really, the HNO_3 peak is caused by evaporation of particulate nitrate formed in the upper PBL (where the conditions of lower temperature and higher relative humidity are favourable to NO_3 formation), and mixed towards the surface by vertical mixing (Curci et al., 2015a; Aan de Brugh et al., 2012). Therefore, the unrealistic afternoon peak of modelled nitric acid should result from a too rapid relaxation of aerosol–gas partitioning to thermodynamic equilibrium (Aan de Brugh et al., 2012).

The behaviour of the simulated NH_4 is related to a modelled trend of NO_3. It is biased high by 0.66 $\mu g\,m^{-3}$ (+66 %). The NH_4 overestimation is related to NH_3 underprediction (Meng et al., 1997).

Similar performances are found in reproducing inorganic aerosols at other Dutch EMEP sites (see Sect. 3.1). Daily SO_4 is simulated with an average correlation (3 stations) of 0.66 and a positive bias of 35 %. WRF-Chem simulates NH_4 with a correlation of 0.82 (4 stations) and a bias of +43 %. Predicted daily NO_3 (measured at only one station) is overestimated by 15 %.

Organic matter is reproduced with a correlation coefficient of 0.75. WRF-Chem reproduces the right concentration during the dry period (the decrease in the wet days) and following recovery. The mean bias is negative by about 0.4 $\mu g\,m^{-3}$ and it is attributable to days from 23 to 26 May. The discussion about the origins of OM bias is given in Sect. 4.3, where we will discuss the model evaluation with aircraft data.

The reader should consider that aerosol composition measurements performed with the AMS are representative of particles with a diameter between roughly 100 and 700 nm, whereas the model is evaluated with aerosol concentration representative of $PM_{2.5}$. Therefore, a bias could be present in the comparison. This means that the bias found for inorganic aerosols could be smaller than that reported above; conversely, the OM bias could be larger than that found.

The model evaluation performed so far is representative of few points in the domain and does not include other aerosol components like black carbon or primary PM. This could limit our understanding of the model behaviour. In or-

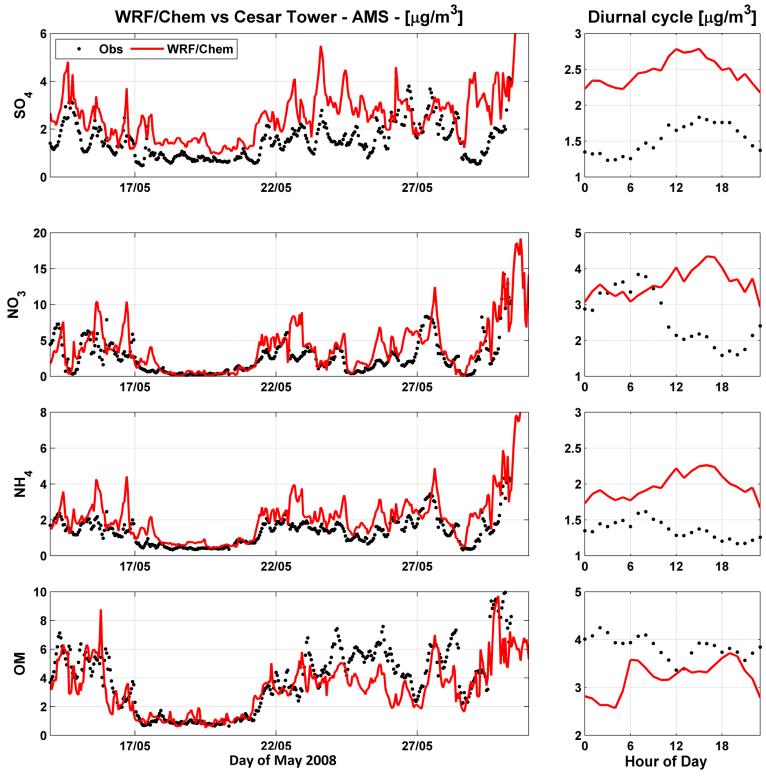

Figure 5. As in Fig. 4, but for aerosol mass speciation at Cesar observatory observed at 60 m height.

der to overcome this shortcoming, WRF-Chem is also compared to daily PM_{10} measurements of the AIRBASE network (Fig. S2). The model captures the daily variations of PM_{10}, the PM_{10} decrease during scavenging days, the consequent recovery to reach back the background PM_{10} concentration, and the PM_{10} enhancement during the long-range transport period. Indeed, the correlations are of 0.72, 0.73, and 0.75 in rural, suburban, and urban zones, respectively. Model bias at rural stations is important in the last days of May 2008; indeed, in these days (28–30 May) it is about $-15\,\mu g\,m^{-3}$ ($-30\,\%$). Conversely, at suburban and urban stations, the model presents a bias for the most part of the days of about 3–4 $\mu g\,m^{-3}$ (5–10 %) that could partly be explained by the missing source of resuspension due to traffic.

The results obtained here are statistically consistent with other modelling studies over Europe (e.g., Lecœur and Signeur, 2013; Zhang et al., 2013b; Balzarini et al., 2015). For example, the results of European annual simulations of Balzarini et al. (2015) exhibited a correlation of 0.48, 0.60, and 0.56 for surface SO_4, NO_3, and NH_4, respectively. During EUCAARI campaign, Athanasopoulou et al. (2013) reported a mean correlation of surface OM with observations of 0.56 and a mean bias of $-0.5\,\mu g\,m^{-3}$, whereas Fountoukis et al. (2014) simulated the OM at Cabauw on May 2008 with a bias of $0.3\,\mu g\,m^{-3}$. Moreover, with regards to surface PM_{10}, our performances are comparable to those found, for example, by Im et al. (2015) over Europe with annual simulations in terms of correlation, but are higher in terms of bias. Comparing PM_{10} concentrations from several models, Im et al. (2015) found correlations of 0.18–0.86 and 0.07–0.82, and bias of about -40 and $-50\,\%$ for rural and urban sites, respectively. This improvement is most likely due to the very high resolution used in this study with respect to the 23 km of Im et al. (2015), since the anthropogenic emissions inventory used is the same here and in the study by Im et al. (2015).

4.3 Aloft aerosol mass concentration

The comparison of WRF-Chem to aircraft data is done by interpolating the model output point by point along the flight track. Observed and modelled aircraft data are presented by using the box plots for planetary boundary layer (PBL) and free troposphere (FT) (see Fig. 6). The height of the PBL was lower than 1600 m during the whole campaign (Crumeyrolle et al., 2013). Therefore, we considered for PBL and FT concentrations the data below and above 1600 m up to 3000–4000 m, respectively. This rough approximation of PBL height could affect the comparison of the model to data.

Figure 6 displays the observed and modelled box plots of the mass concentration of SO_4, NO_3, NH_4, and OM for PBL and FT. Their mean value, standard deviation, relative mass fraction, and correlation coefficients, averaged over the whole period of interest, are reported in Table 3.

Table 3. Observed and modelled mean values, standard deviations, and relative number (expressed as percentage) of aerosol species, number of aerosol particles, cloud condensation nuclei, over the whole period of the aircraft campaign in boundary layer and free troposphere.

	Boundary layer			Free troposphere		
	Observation	WRF-Chem	r	Observation	WRF-Chem	r
SO_4 ($\mu g\,m^{-3}$)	3.1 ± 2.4 (19 %)	3.2 ± 2.1 (24 %)	0.39	2.6 ± 2.0 (29 %)	2.5 ± 1.2 (38 %)	0.23
NO_3 ($\mu g\,m^{-3}$)	4.5 ± 5.4 (28 %)	4.6 ± 5.1 (34 %)	0.47	1.3 ± 3.0 (14 %)	1.5 ± 2.7 (23 %)	0.44
NH_4 ($\mu g\,m^{-3}$)	2.6 ± 2.2 (16 %)	2.4 ± 2.1 (19 %)	0.43	1.4 ± 1.5 (16 %)	1.2 ± 1.2 (19 %)	0.42
OM ($\mu g\,m^{-3}$)	6.1 ± 5.8 (37 %)	3.0 ± 2.6 (23 %)	0.67	3.7 ± 4.5 (41 %)	1.3 ± 1.4 (20 %)	0.52
$PM_{2.5}$ ($\mu g\,m^{-3}$)	23 ± 13	16 ± 10	0.75	19 ± 17	12 ± 9	0.80
CN ($10^3\,\#\,cm^{-3}$)	6.7 ± 5.0	9.4 ± 5.4	0.40	1.0 ± 1.1	1.7 ± 2.8	0.74
CCN ($10^3\,\#\,cm^{-3}$)	0.6 ± 0.5	0.9 ± 0.8	0.45	0.3 ± 0.3	0.3 ± 0.3	0.73

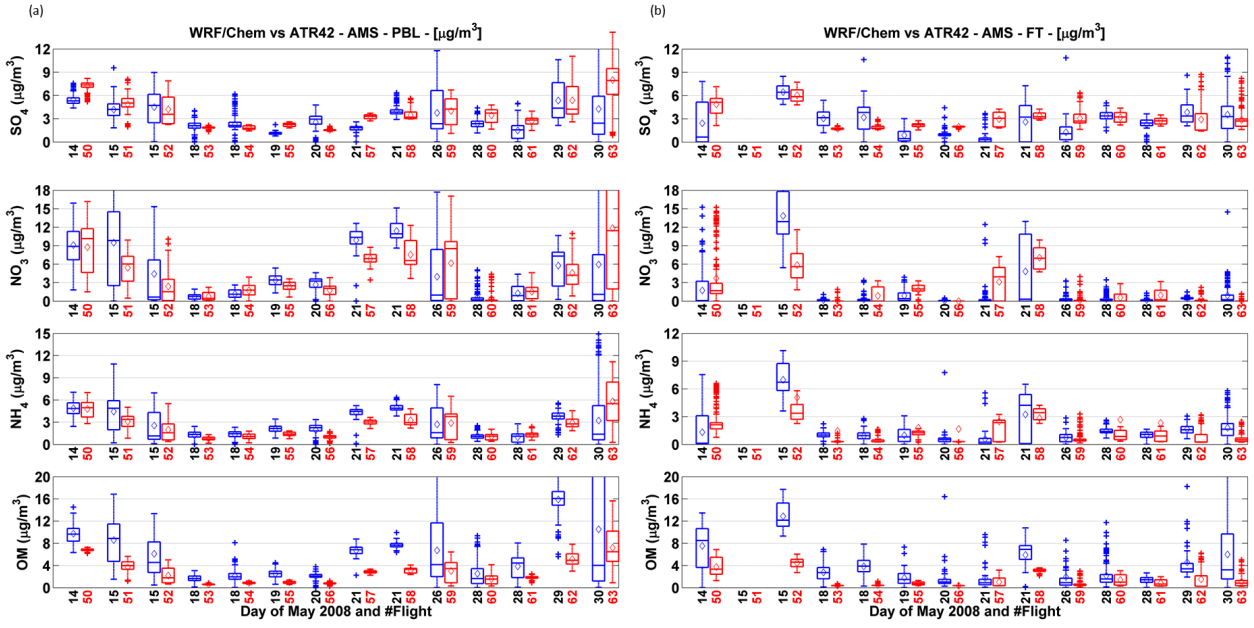

Figure 6. Box plot of SO_4, NO_3, NH_4, and OM mass concentrations measured by AMS aboard the ATR-42 (blue) and simulated by WRF-Chem (red) within boundary layer **(a)** and free troposphere **(b)**. The x axis reports the day of May 2008 (black) and the number of the research flight (red). The whisker plots denote median, 25th and 75th percentiles, 1.5 × (inter-quartile range), and outliers. The squares represent the mean values.

The average concentrations of inorganic aerosols show little absolute error (2–8 %) with respect to the observations in the PBL, while the NO_3 and NH_4 mean concentration presents a bias of +14 and +20 % (+0.3 and +0.2 $\mu g\,m^{-3}$), respectively, in the FT. The mean OM mass is biased low by a factor of 2 and 3 in the PBL and FT, respectively. The correlation coefficients of SO_4, NO_3, NH_4, and OM are 0.39, 0.47, 0.43, 0.67 in the PBL and 0.23, 0.44, 0.42, 0.53 in the FT. These performances are comparable with those found with WRF-Chem (but with a different chemistry package) in California by Fast et al. (2014). They reported an absolute mean bias of about 0.01–0.2, 0.03–0.6, 0.1–0.45, 0.2–0.57 $\mu g\,m^{-3}$ and a mean correlation of 0.42, 0.45, 0.44, and 0.72 for SO_4, NO_3, NH_4, and OM, respectively.

Although the predicted aerosol mass of each species is within the range of the observed values for most of the flights used in this study (see Fig. 4), the model does not capture the full range of the measured concentrations. This assertion is made quantitative by the standard deviations reported in Table 3. The predicted standard deviations for each species are lower than observed. In the PBL, the observed and modelled standard deviations differ by 4–10 % for inorganic ions and 55 % for OM. In the FT, the differences are higher than in the PBL. The model predicts standard deviations lower than 10–40 % for inorganic particles and lower than 65 % for organic matter with respect to the measurements.

For the purpose of this analysis, it is also interesting to explore how the model reproduces the relative fraction of

aerosol mass species with altitude (see Table 3). WRF-Chem overpredicts the relative fraction of the SO_4 and NO_3 by few percent in the PBL and about 10 % in FT, while the relative mass of NH_4 is overestimated by 3 % along the whole profile. The relative amount of OM is underpredicted by about 20 % in both PBL and FT. The decrease of relative amount of NO_3 and increase of SO_4 with altitude is captured by the model. The modelled relative mass of NH_4 and OM is near constant with altitude as well as in the observations.

Looking at the individual flights, it is possible to note how the model captures the aerosol mass trend as a function of the synoptic frame in both the PBL and FT, during the dry period, scavenging days, and dust period characterized by southerly wind and passage of several fronts. The FT is a layer mainly affected by long-range transport and cloud contamination. Therefore, the relative small bias in simulating aerosol inorganic mass in FT means that the model resolves quite correctly the large-scale transport and processes related to clouds.

Nevertheless, it should be noted that SO_4 is overestimated for 8 out of 14 RFs, while NO_3 and NH_4 are underpredicted for 7–8 out of 14 RF. This SO_4 overprediction is attributable to the SO_2 excess and to a potential overproduction within the cloud chemistry scheme. The negative bias of NO_3 and NH_4 could be explained by a low NH_3 regime, that limits the formation of the ammonium–nitrate.

The simulated OM concentration is always at the lower end of the observed variability. Several factors may explain this systematic bias. First of all, our simulations do not include the processing of organic compounds in aqueous chemistry. SOA may be produced in the clouds (Hallquist et al., 2009). Modelling studies suggest that the contribution of cloud chemistry to SOA budget is almost as much as the mass formed from the gas phase (Ervens et al., 2011). OM prediction is also affected by meteorological errors. Bei et al. (2012) found that the uncertainties in meteorological initial conditions have a significant impact on the simulations of the peaks, horizontal distribution, and temporal variation of SOA. The same authors demonstrated that the spread of the simulated peaks can reach up to 4.0 $\mu g\,m^{-3}$. Other uncertainties may be related to the VBS formulation. The SOA formation pathway is one these, indeed halving the SOA yields the concentration of SOA decreases by 30 % (Ahmadov et al., 2012). Moreover, the assumption on the deposition velocity of the OCVs may play an important role in the uncertainties of SOA production. The OCV deposition velocity in the version of the VBS implemented in WRF-Chem by Ahmadov et al. (2012) is proportional to the deposition velocity of the HNO_3. The proportionality constant is a tunable parameter and in this work is set to the default value of 0.25. WRF-Chem prediction of SOA mass is very sensitive to the choice of the proportionality constant (Ahmadov et al., 2012). Previous studies have shown that SOA concentration is highly sensitive to the treatment of the deposition velocity of OCVs (Bessagnet et al., 2010; Knote et al., 2015b). Finally, we note

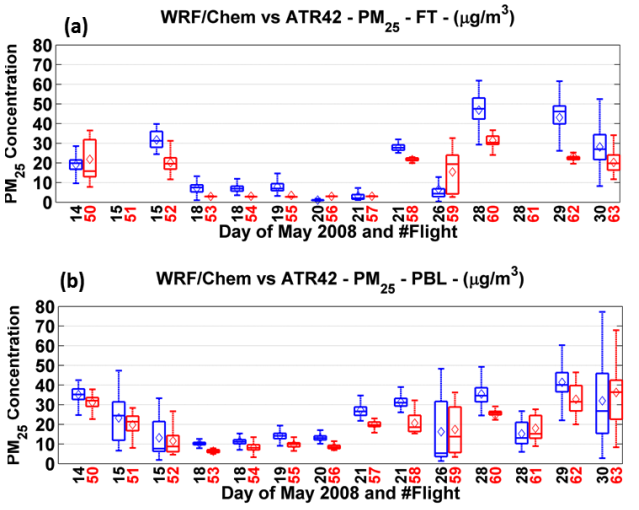

Figure 7. Same as Fig. 6 but for observed and simulated $PM_{2.5}$ mass concentrations. The blue colour represents the observations, while the model is displayed in red colour.

that OM bias could be partially explained by the uncertainties in the anthropogenic emissions (e.g. bias or spatial distribution) of primary organic carbon and in the factor 1.6 used to convert them to POM (Turpin and Lim, 2001). The reader should also consider that the uncertainties in POM simulation affect the SOA formation. Indeed, the partition between OCV and SOA used in the VBS approach depends on the total OM (Eq. 1 of Ahmadov et al., 2012); thus, if POM is underpredicted the resulting SOA could be underestimated.

In order to have a more complete overview of the model skill in reproducing the upper air aerosol mass concentration, we also compare the observed and modelled $PM_{2.5}$. Figure 7 shows measured and predicted box plots of the $PM_{2.5}$ concentration in PBL and FT. Modelled $PM_{2.5}$ is in the range of the observed values within the PBL expect during the wet scavenging period when it is at the lower end of the observations. In FT, conversely, predicted $PM_{2.5}$ is at the lower end of the observed profiles for the most part of the flights. The comparison between modelled and observed $PM_{2.5}$ concentration within PBL and FT show good correlations (0.75 and 0.80, respectively).

Model correlation with observations is high, 0.75 and 0.80 in PBL and FT, respectively. The absolute mean bias is $-7\,\mu g\,m^{-3}$ (30–35 %) in both PBL and FT.

Although the box plot and statistical summary (Table 3) provide significant information on the model performances, the model skills in reproducing vertical profiles of aerosol properties need to be evaluated. Therefore, we also look at model vertical profiles along the flight tracks. As an example, we have chosen the 14 May 2008 (RF50) for two reasons: first, there is a relatively large contribution of OM, SOA (70–85 % of OM), and CCN (see Fig. 10), and second, it is a day of high pressure; thus, the interpretation of the re-

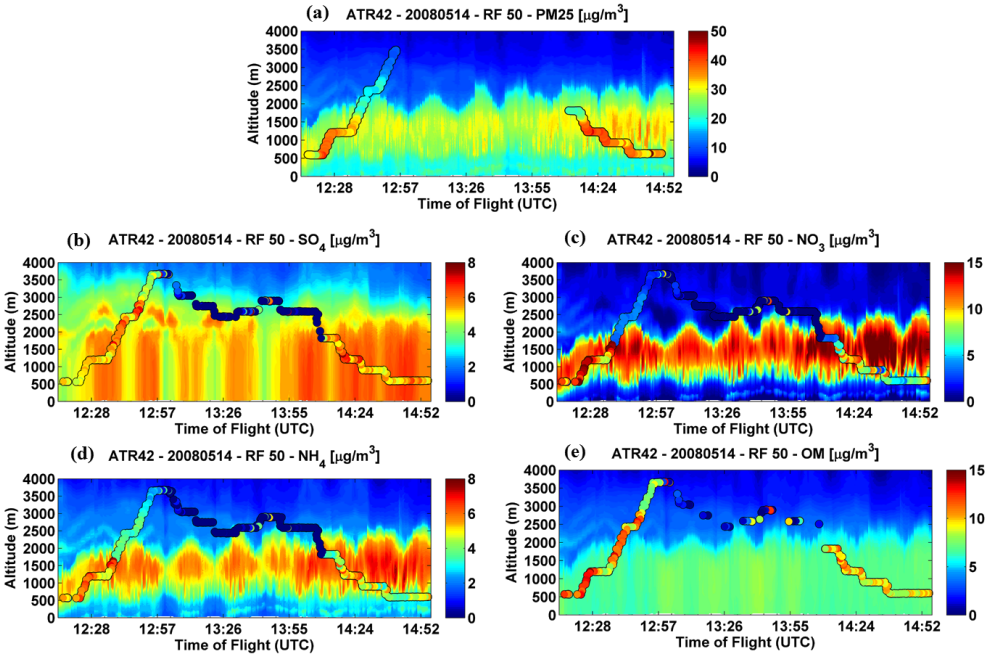

Figure 8. Vertical profiles (shadow) along the flight track of 14 May (RF50) of modelled $PM_{2.5}$ **(a)**, SO_4 **(b)**, NO_3 **(c)**, NH_4 **(d)**, and OM **(e)**. The circles are the measurements collected aboard the ATR42.

sults is not complicated by cloud processes. Figure 8 displays the comparison of modelled vertical profiles of $PM_{2.5}$, SO_4, NO_3, NH_4, and OM along the flight track and measurements. WRF-Chem captures several features present in the aircraft observations. Both observed and modelled $PM_{2.5}$ exhibit a maximum in a layer between 500 and about 2000 m. The model predicts the inhomogeneity of the chemical secondary species of $PM_{2.5}$ also displayed in the observations: SO_4 and OM concentrations are relatively homogeneous within the PBL, whereas NO_3 and NH_4 show enhanced concentrations in the upper levels of the PBL. For completeness, we note that primary $PM_{2.5}$ components (not shown) have their maximum close to the surface (first 500 m) and are diluted throughout the PBL. These results are qualitatively similar to those found by Curci et al. (2015a) above Milan (Italy).

4.4 Aloft aerosol particles

The comparison of WRF-Chem output with aircraft measurements of the number concentration of condensation nuclei (CN) and of CCN at 0.2 % of supersaturation is done by using the box plots as for aerosol mass. In this case the modelled and measured data are smoothed by using a 10 s running mean.

Figure 9 reports the comparison of observed and modelled CN within PBL and FT. The measured and predicted average, standard deviation, and correlation of the CN number over the whole period of our analysis are reported in Table 3.

The model resolves the decrease of a factor of 5–6 of CN concentration between the PBL and the FT. The differences

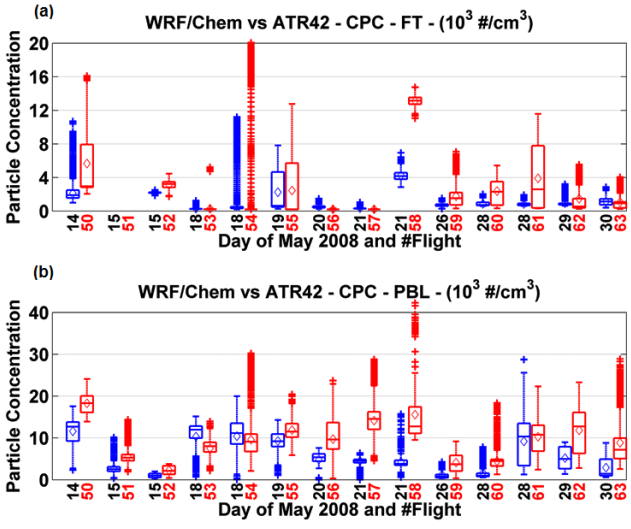

Figure 9. Same as Fig. 6 but for observed and simulated condensation nuclei (CN) concentrations. The blue colour represents the observations while the model is displayed in red colour.

in simulated concentrations between land and sea (RF51 and 52) are also captured by the modelling system. Nevertheless, WRF-Chem overestimates, on average, the observed CN by a factor of 1.4 within PBL and 1.7 within the FT. The bias is less pronounced above the sea during the RF51 and RF52, where the anthropogenic sources are less important. Moreover, it should be noted that in some cases, for example during the RF56, 57, and 58, the predicted CN are completely

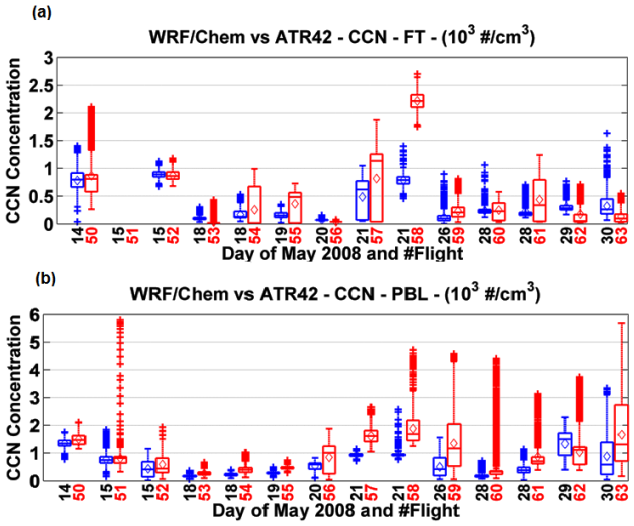

Figure 10. Same as Fig. 6 but for observed and simulated cloud condensation nuclei (CCN) concentrations at 0.2 % of supersaturation. The blue colour represents the observations, the model is displayed in red colour.

outside the range of the observed values. In these cases the predicted CN are biased high by about a factor of 2–3. Predicted CN concentration shows a higher variability than measured, especially in the free troposphere where the difference of modelled standard deviation is biased high by 155 %. Anyway, the modelled CN concentration correlates well with the observed one (0.40 and 0.74 in PBL and FT, respectively). These values are consistent with the 0.61 found by Luo and Yu (2011) studying the new particle formation and its contribution to CN with a version of WRF-Chem including an advanced aerosol microphysical model.

Figure 10 shows the comparison of observed and modelled CCN at 0.2 % of supersaturation. The measured and predicted average and standard deviation of CCN are showed in Table 3. The bias of simulated $CCN_{0.2}$ appears more contained with respect to CN prediction, especially in the free troposphere. Figure S3 shows the comparison of the modelled vertical profile of CCN along the flight track of 14 May and observed CCN aboard the ATR42. WRF-Chem predicts relatively homogeneous profile of CCN in the PBL also shown by observations.

The aerosol particles that mostly contribute to the CCN number are those of accumulation and coarse modes, and accumulation and coarse-mode particles are also the major contributor to $PM_{2.5}$ mass concentrations. Since $PM_{2.5}$ is underestimated and CCN overestimated, CCN bias cannot depend on model errors in $PM_{2.5}$. The major uncertainties in predicted CCN arise from aerosol nucleation rate and primary emissions (Lee et al., 2013). Direct emission of aerosol particles is the key factor for CCN production in the PBL and near particle sources (Spracklen et al., 2006), and account for 55 % of the total global production (Merikanto et al., 2009). On the other hand, nucleation and subsequent growth up to CCN size is an important mechanism of CCN formation in many parts of the atmosphere (Sotiropoulou et al., 2006). Using several nucleation parameterizations, Pierce and Adams (2009) showed that CCN on average varies by up to 12 % within the PBL. At the same time, they also found that varying by a factor of 3 the primary emissions, the CCN mean changes by 40 % in the PBL. On the basis of these argumentations and the correlation between predicted and observed CN being larger in the FT than in PBL (i.e. far from anthropogenic sources), we may speculate that the errors in the CCN prediction arise mainly from the uncertainties in the primary emissions of the aerosol particles and in their distribution in the log-normal modes.

The analysis of CCN efficiency reveals other interesting features in the model behaviour. The CCN efficiency is given by the CCN / CN ratio and represents the ability of aerosol particles to nucleate cloud droplets (Andreae and Rosenfeld, 2008). CCN efficiency observed during the studied RFs is in the range of 0.02–0.33 for PBL and 0.18–0.41 in the FT, while the model predicts values of 0.03–0.17 and 0.04–0.18 for PBL and FT, respectively. In other words, WRF-Chem underestimates the CCN efficiency by a factor of 1.5 and 3.8 within the PBL and FT, respectively. Moreover, the modelled CCN efficiency, contrary to the observation, shows almost the same range of values within the PBL and within the FT.

The so-calculated and modelled CCN efficiencies could be underestimated. In general, the CCN efficiency should be computed with the aerosol population with size larger than the minimum activation diameter (Asmi et al., 2012). The latter depends on the aerosol type and ranges from about 50 to 125 nm. We calculated the observed CCN / CN ratio with the measurements of CPC 3010 which gives the total number of particles larger than 15 nm, and the modelled CCN fraction is calculated with total particle number given by the sum of the three modes of the log-normal distribution (Aitken, accumulation and coarse). In order to better characterize the relationship between CCN and the corresponding aerosol population in the model, predicted CCN efficiency was also calculated with particles of the accumulation and coarse modes (the most favoured particles to act as CCN), and it was qualitatively compared to observed efficiency during the IMPACT campaign computed with particles larger than 100 nm. Observed values of CCN efficiency are in the range of 0.28–0.4 and 0.38–0.6 in the PBL and FT (Crumeyrolle et al., 2013), respectively. The simulated CCN fraction calculated with the particles of the accumulation and coarse modes, is always underestimated with respect to the observations, and it is in the range of 0.17–0.3 in PBL and 0.23–0.36 in FT. The model deficiency in simulating the CCN / CN ratio could be attributable to the uncertainties in geometrical diameter and bulk hygroscopicity of the log-normal modes, and updraft velocity that lead to error in the prediction of minimum activation diameter of each mode.

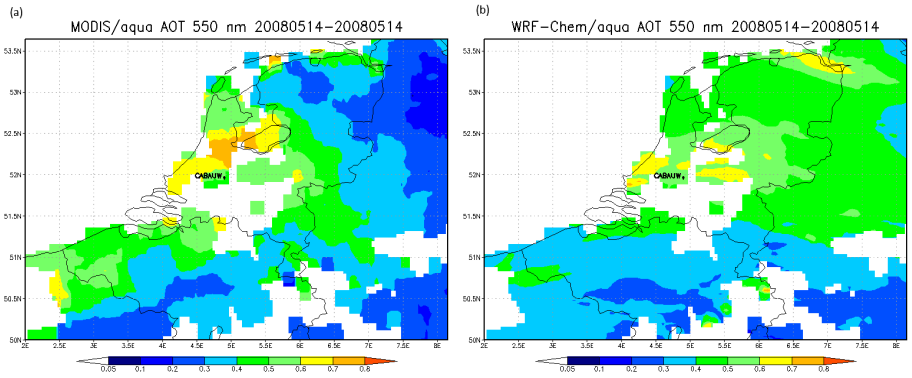

Figure 11. Aerosol optical thickness at 500 nm from MODIS-Aqua **(a)** and WRF-Chem simulations **(b)** on 14 May 2008.

4.5 Comparison with MODIS data

WRF-Chem output was also compared to AOT, cloud microphysical, and optical properties retrieved by MODIS-Aqua.

Figure 11 shows the comparison between the AOT at 550 nm measured by MODIS and the corresponding AOT predicted by the model during the high-pressure period on 14 May 2008. WRF-Chem reproduces the spatial distribution of observed AOT, such as the lowest values in the southern part of the domain or the highest values around Cabauw, but underestimates the strong gradient between the eastern boundary and the centre of the domain. The model overestimates the regional mean of AOT; indeed, the domain averages are 0.38 ± 0.12 and 0.42 ± 0.10 for MODIS and WRF-Chem data, respectively. Unfortunately, good coverage of the D3 domain by MODIS was achieved only on 1 day (14 May 2008), this does not allow us to have a general overview of model skill in predicting AOT. In general, model intercomparisons revealed that a large part of the uncertainties in simulating the AOT arises from the assumption on the mixing state. For example, AOT computed with external mixing is larger by 30–35 % of that calculated with internal mixing assumption (Curci et al., 2015b). For typical atmospheric particle sizes and in the visible wavelength range, the AOT is then expected to be lower under internal mixing assumption (that is the assumption done in this work). Moreover, a 10 % error in predicting AOT may be attributable to the choice of species density, refractive index, and hygroscopic growth factor (Curci et al., 2015b).

As the WRF microphysics scheme accounts for aerosols only within liquid clouds, comparison among predicted cloud optical and microphysical properties with MODIS data was done separately for liquid, excluding mixed clouds. Top liquid cloud R_e was calculated from liquid water content (LWC) and cloud droplet number concentration predicted by WRF-Chem. Liquid water path (LWP) was calculated by vertically integrating liquid cloud mixing ratios (water and rain water), while liquid COT was estimated from LWC and R_e. Since MODIS L2 data provide the total cloud water path (CWP), combined effective radius for all cloud types and total (water and ice) COT, the observed contribution to the liquid water cloud was separated by using the retrieved top cloud phase, i.e. were discarded mixed clouds.

The comparison between the predicted and observed R_e, LWP, and liquid COT was done in the scavenging background and long-range transport periods in the days when MODIS cloudy pixel coverage was larger than 60 %. Figure 12 shows the comparison of the averaged values for 17–19 May 2008 period (1P). The same comparison has been done on averaged values for 25–27 (2P) and 28–30 May (3P) and are reported in the Supplement (Figs. S4 and S5). WRF-Chem reproduces several features of the liquid cloud systems during 1P: the liquid cloud distribution, the maximum values of R_e close to the coast, maximum of LWP, and liquid COT on the centre and at north-east of the domain. However, model results present a larger spatial extension of liquid water cloud highest values off the Dutch and Belgian coasts not observed in the MODIS data. During 2P the structure of the cloud system is not completely reproduced by the model. Although R_e value magnitude is captured above the sea, WRF-Chem underestimates the cloud droplet dimension on the land. Therefore, LWP and liquid COT structure on the sea is resolved by the model, whereas on the land they are too small compared to the observations. Finally, the model reproduces the average structure of the cloud system in 3P, but LWP and liquid COT are overestimated on the western part of the domain.

As shown in Table 4, R_e values averaged over the entire domain are underestimated by the model by a factor of about 1.5 during all three periods of interest. LWP, values averaged over the entire domain, is also overestimated in all three cases by a factor of 1.1, 1.3, and 1.6 for 1P, 2P, and 3P, respectively. The R_e (LWP) underprediction (overestimation) may be due to the overestimation of droplet number concentration that stems from overestimation of CN. Another reason that could explain the positive bias of modelled LWP is the inefficient autoconversion of cloud water to rain, typical of the Morrison microphysical scheme (Saide et al., 2012). The consequence

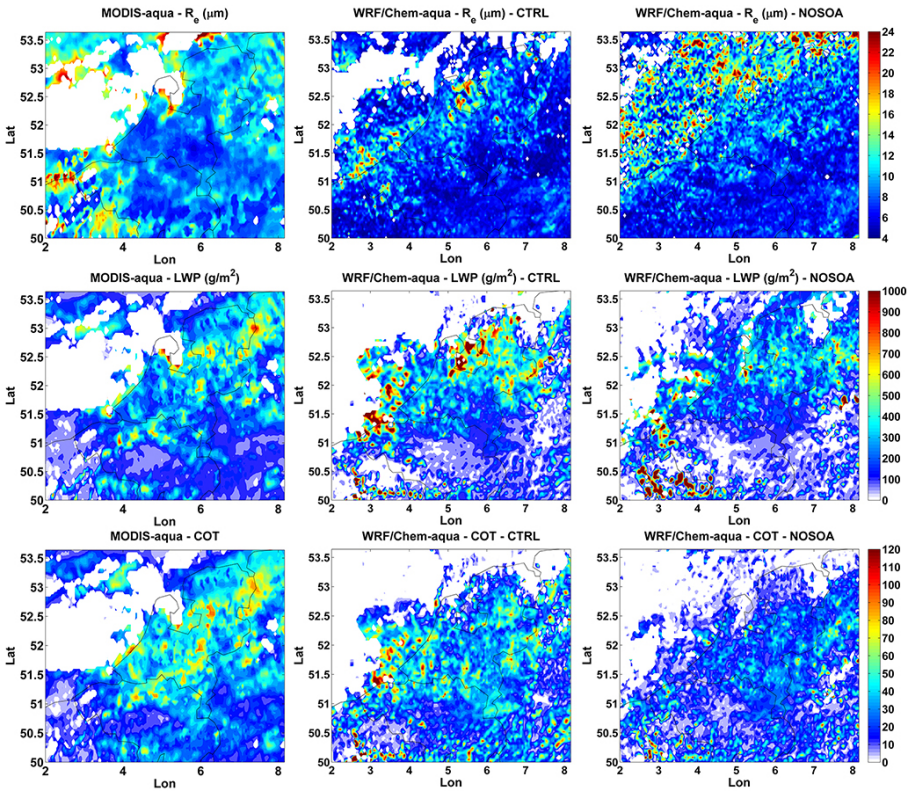

Figure 12. The 17–19 May 2008 averages of droplet effective radius at cloud top (first row), liquid water path (second row), and liquid cloud optical thickness (third row), retrieved using MODIS-aqua observations (first column), predicted by model in the references run (CTRL, second columns) and sensitivity test without SOA (NOSOA, third column).

of the negative (positive) of R_e (LWP) is the overestimation of average liquid COT by few percent for 1P and 3P, and 42 % for 3P.

The biases found here are quite different from the WRF-Chem study by Yang et al. (2011) on the modelling of marine stratocumulus in the south-east Pacific. They have shown a bias of +30 % in reproducing the COT, while LWP was underestimated by a factor of 1.3. The reader should note that in Yang et al. (2011), the aerosol model adopted was different from the one used here and SOA formation was not included at all.

Figure 13 displays the distribution functions (DF) of R_e, LWP, and liquid COT for 1P. The DF for 2P and 3P are reported in the Supplement (Figs. S6 and S7). In all three periods analysed, the model captures the frequency of large droplets ($R_e > 18$–20 μm), underestimates the number of small droplets (8–$10 < R_e < 18$–20 μm), and overestimates the frequency of very small cloud droplets ($R_e < 8$–10 μm) by more 30 %. Whereas DF of the observed R_e presents the maximum in the range of 8–13 μm, modelled DF shows the maximum values in correspondence of the droplets with size less than 7–8 μm. WRF-Chem captures the shape of the distribution functions of LWP and liquid COT, but underestimates the maximum and overestimates the higher and lower end of the distributions. Both variables show a variability higher than the observations. The predicted standard deviations (Table 4) are about 2–3 and 1.5 times larger than those observed for LWP and liquid COT, respectively. This probably stems from the large variability in simulated CCN.

Now it is interesting to analyse the model behaviour in reproducing the total CWP and COT given by contribution of all cloud phases. Modelled CWP was calculated by vertically integrating all cloud mixing ratios (water, rainwater, ice, snow, and graupel). Predicted COT is given by the contribution of the liquid water and ice. The contribution of the liquid water was calculated as described above for liquid water cloud. The contribution of ice phase to COT was calculated following Ebert and Curry (1992).

Figure 14 displays the comparison between observed and predicted CWP and COT in P1, whereas the same figures for P2 and P3 are reported in the Supplement (Figs. S8 and S9). Although for all three cases, the model reproduces with good approximation the shape and localizations of the cloud systems, CWP and COT are systematically overestimated (except COT in P2). As shown in Table 5, the predicted domain average of CWP presents, indeed, a bias of 62, 41, and 80 % for P1, P2, and P3, respectively, whereas the bias of COT is about 15 % in P1 and P3.

Table 4. MODIS and modelled mean values and standard deviations of droplet effective radius at cloud top, liquid cloud water path, and liquid cloud optical thickness, on 17–19, 25–27, and 28–30 May 2008.

	R_e (μm)			LWP (g m^{-2})			COT		
	MODIS	CTRL	NOSOA	MODIS	CTRL	NOSOA	MODIS	CTRL	NOSOA
17–19 May	10.2 ± 3.5	7.5 ± 3.5	8.5 ± 4.3	230 ± 343	242 ± 343	208 ± 352	32 ± 22	33 ± 33	21 ± 24
25–27 May	13.7 ± 3.7	9.1 ± 4.4	9.8 ± 4.9	200 ± 166	256 ± 502	273 ± 480	22 ± 19	23 ± 30	21 ± 27
28–30 May	10.7 ± 3.9	8.4 ± 4.1	7.8 ± 3.6	141 ± 128	224 ± 327	243 ± 447	19 ± 14	27 ± 27	24 ± 30

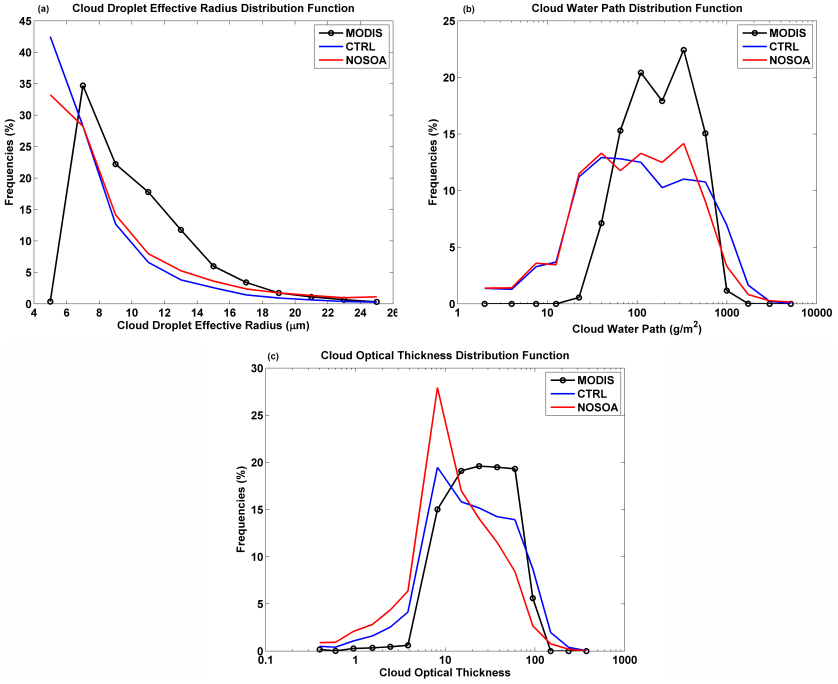

Figure 13. The 17–19 May 2008 averages of observed and simulated distribution function of droplet effective radius at cloud top **(a)**, liquid water path **(b)**, and liquid cloud optical thickness **(c)**. The black line represents the observations retrieved by MODIS, blue and red colours correspond to model predictions from the reference run (CTRL) and sensitivity test without SOA (NOSOA), respectively.

At this point of the analysis, although the aerosol–cloud interaction is a very complex non-linear process, we are able to relate the model error in aerosol particles to the uncertainties in cloud prediction. The overestimation of CN leads to overprediction of the CCN. Higher number of CCN means clouds with a higher number of cloud droplets, higher water content, smaller droplets, and clouds optically deeper.

In addition to the uncertainties in aerosol particle simulation, one typical source of error in the prediction of cloud fields is the choices related to the model setup. For example Otkin and Greenwald (2008) found a strong sensitivity of cloud properties while evaluating the response of the WRF model to the permutation of several PBL and cloud microphysical schemes. Moreover, the same authors have shown that the low level clouds are sensitive to PBL parameterization, whereas the upper level clouds are sensitive to both PBL and microphysics schemes.

One element that may affect the model–satellite comparison are the uncertainties associated with the retrieval. For example, in South Pacific stratocumulus, MODIS overestimates the droplet effective radius by 13–20 % with respect to concomitant in situ measurements (Painemal and Zuidema, 2011; King et al., 2013). The overestimation of COT by MODIS results in the overestimation of CWP (King et al., 2013). Henrich et al. (2010) have shown systematic differences between MODIS data and in situ observations. Indeed, analysing a system of thin cumulus clouds during the EUCAARI campaign, they also found that MODIS overestimates the droplet effective radius by a factor of 2–3 and COT is 2–3 times lower than the in situ measurements.

Table 5. MODIS and modelled mean values and standard deviations of cloud water path and cloud optical thickness of clouds in all phases, on 17–19, 25–27, and 28–30 May 2008.

	CWP ($g\,m^{-2}$)			COT		
	MODIS-Aqua	CTRL	NOSOA	MODIS-Aqua	CTRL	NOSOA
17–19 May	207 ± 203	336 ± 531	218 ± 359	26 ± 20	30 ± 33	19 ± 23
25–27 May	235 ± 182	331 ± 533	244 ± 418	21 ± 16	17 ± 23	16 ± 21
28–30 May	206 ± 201	370 ± 714	262 ± 523	21 ± 16	24 ± 26	21 ± 27

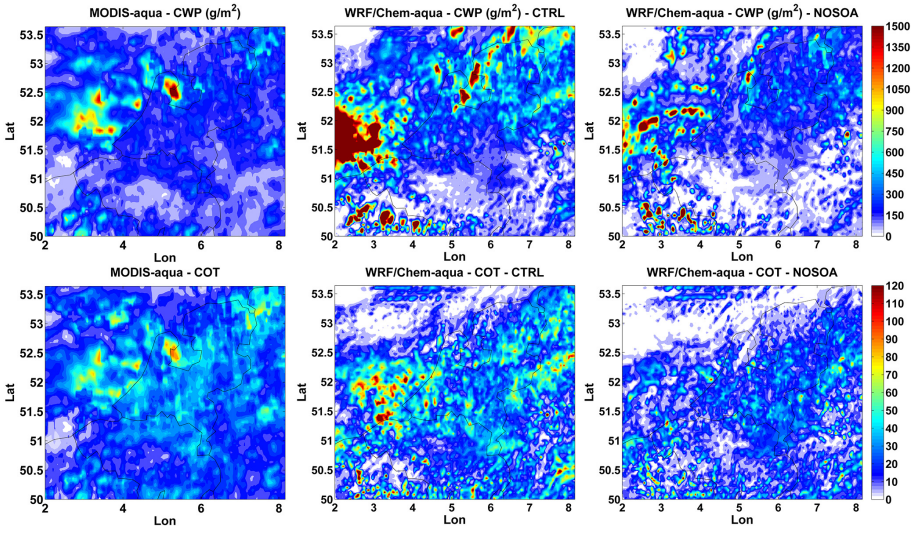

Figure 14. As in Fig. 12, but for clouds in mixed phase.

5 Impact of SOA particles on cloud prediction

The last part of this study focussed on the evaluation of the impact of SOA on the simulation of cloud fields. We performed sensitivity simulations during P1, P2, and P3 without the SOA (NOSOA), and compared them to the reference run (CTRL) discussed so far. NOSOA runs are carried out only in the higher resolution domain (D3). The simulations of all three periods are initialized at 00:00 UTC with the same meteorological and chemical input data used for CTRL, except chemical initial conditions that are restarted by a previous NOSOA run. Each period is preceded by 30 h of simulation used as spin-up for D3 chemistry. The sensitivity simulation is performed zeroing the arrays pertaining to SOA. Thus, the SOA fields are not affected by incoming SOA from domain boundaries or by local production. We did not perform the sensitivity tests with the SORGAM option because this model produces very little SOA mass concentrations (Grell at al., 2005; McKeen et al., 2007; Tuccella et al., 2012). Therefore, we may assume that simulations with SORGAM and without SOA (in VBS option) are roughly equivalent. The advantage of this assumption is that the model is forced with the same initial meteorological conditions and boundary meteorological and chemical conditions as the CTRL simulation. The use of SORGAM would require running the model on all three domains, leading to different results on D2 which is used to initialize D3. Finally, this would introduce dependencies on the D3 input data making the comparison not directly comparable to the CTRL run.

The comparisons of R_e, LWP, and liquid COT simulated in CTRL and NOSOA runs with MODIS data are reported in Figs. 12, S4, and S5. In general, the average spatial pattern of these three variables is captured better by the CTRL simulation with respect to the NOSOA run, especially in P1. Figures 13, S6, and S7 display the comparison between DFs of the cloud properties simulated by CTRL and NOSOA runs with those retrieved with the MODIS observations. The domain averages for each variable are reported in Table 4. NOSOA runs show a domain averaged R_e larger than CTRL. DFs of the LWP are different between the runs, but it is not clear if there are improvements in CTRL with respect to the NOSOA run. Only the domain averages allow one to establish that LWP values predicted by CTRL run are closer to the observed means than NOSOA. The presence of SOA in the numerical prediction improves the DF of liquid COT with respect to NOSOA simulation in P1 and P3, whereas there are no differences during P2. NOSOA has 10 and 3 % more op-

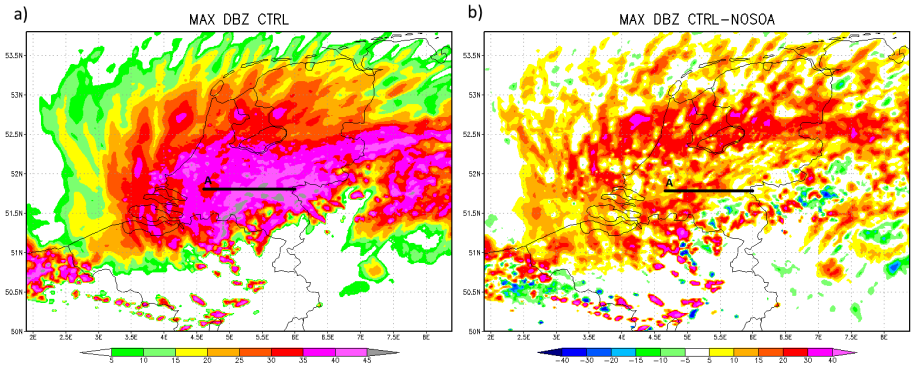

Figure 15. Maximum dBZ at 06:00 UTC of 17 May for CTRL run **(a)** and difference of maximum dBZ between CTRL and NOSOA simulations **(b)**. The solid black line represents the cross section A used to plot vertical profiles reported in Fig. 13.

tically thin liquid clouds (liquid COT < 40) with respect to CTRL in P1 and P3, respectively.

Figures 14, S8, and S9 report the comparison of modelled CWP and COT of all cloud phases predict in CTRL and sensitivity runs with MODIS data. As well as for liquid phase, including SOA aerosol particles in the runs, the WRF-Chem skills to reproduce the observed pattern of observed CWP and COT increase. As shown in Table 5, domain-averaged CWP and COT are larger up to about 50 % in CTRL with respect to NOSOA.

Now it is interesting to explore the impact of SOA on the vertical structure of the cloud fields. As an example we chose the 17 May because around 06:00 UTC a frontal system associated with a trough from the North Sea crossed the Benelux area (Fig. S10). In both runs, some isolated and shallow clouds form during the night. When the cold front reaches Benelux around 05:00–06:00 UTC, a low pressure centre forms (Fig. S11). The winds rotate around the low pressure with speeds up to 14 m s^{-1} at a height of 925 hPa (Fig. S12). A convective system develops around the vortex. Figure 15 shows the maximum radar reflectivity (maximum dBZ) at 06:00 UTC for CTRL simulation, and the difference of maximum dBZ between CTRL and NOSOA runs. In general, the echo is larger for the run with SOA; i.e. the intensity of the storm is stronger in the CTRL run. Figures 16 and 17 show the vertical fields of $PM_{2.5}$ mass, vertical wind, liquid and frozen hydrometeor for both runs in cross section A displayed in Fig. 15. These differences between both simulations (CTRL-NOSOA) along cross section A, are also displayed in Figs. 16 and 17. The convection appears to be stronger in the control simulation, with a larger number of hydrometeors and stronger updrafts and downdrafts. The larger differences in the simulated fields of vertical wind and hydrometeors occur in the same location where the enhancement of $PM_{2.5}$ mass at cloud base occurs (950–900 hPa), roughly at the distance of 5–15 and 40–90 km away of the origin of the cross section A (Figs. 16 and 17). The results should be taken with caution because the aerosol–cloud interaction is treated only for liquid clouds, the interaction of aerosol with ice phase is still missing in the model. Although the aerosol–cloud interaction is a non-linear process, it is possible to give an interpretation of the results with the conceptual model for cloud invigoration proposed by Rosenfeld et al. (2008). The larger number of CCN in CTRL may curb the autoconversion rate of droplets to raindrops; therefore, the beginning of precipitation may be delayed with respect to NOSOA. This delay leads to a larger amount of condensed water that crosses the freezing level and forms ice hydrometeors. The freezing process warms the higher layers of the cloud through release of latent heat, whereas the melting process due to the falling of ice cools the lower levels. This thermodynamic disequilibrium enhances the upward transport of heat. The enhanced conversion of CAPE to kinetic energy may yield the cloud invigoration found in the CTRL simulation.

6 Summary and conclusions

Secondary organic aerosol particles play an important role in aerosol–cloud–radiation interaction because they contribute to the global budget of radiation and cloud condensation nuclei (CCN). The introduction of SOA particles in numerical simulations has the potential to reduce the uncertainties on the prediction of meteorological fields and air quality. To this aim, a parameterization for SOA production based on the recent VBS approach was coupled with microphysics and radiative schemes in the WRF-Chem community model.

The performance of the updated model at cloud resolving scale (2 km horizontal resolution) was evaluated using ground- and aircraft-based measurements collected during the IMPACT-EUCAARI campaign and the data from the MODIS satellite instrument. The study focuses on the Benelux area, around the supersite of Cabauw, from 14 to 30 May 2008. The analysed period was characterized by a few days of high pressure (14–15 May), followed by a scavenged background situation (17–20 May), and finally

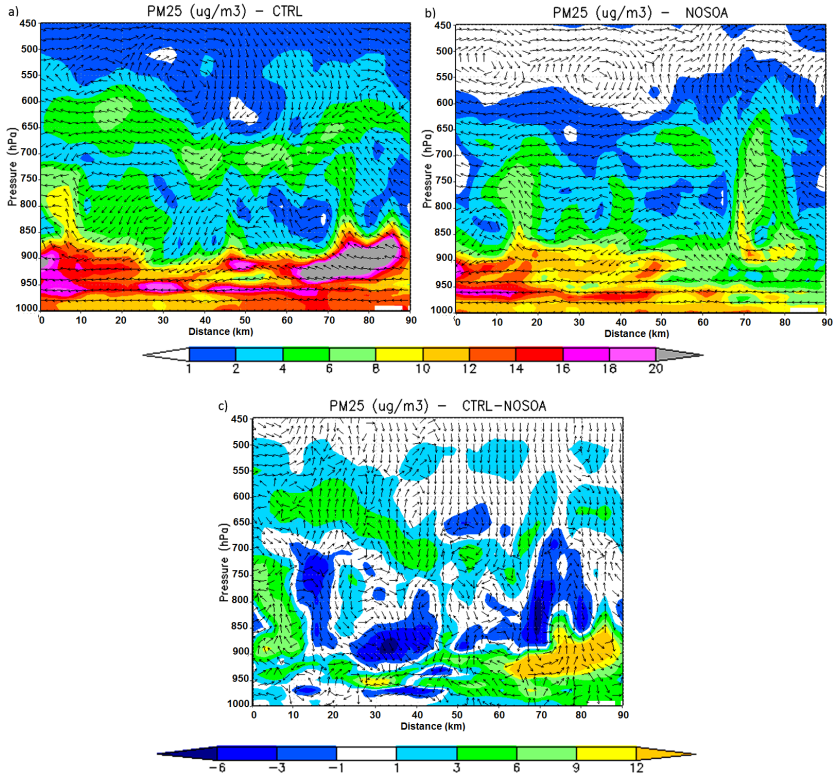

Figure 16. Vertical profile of $PM_{2.5}$ mass (colour) and wind (vector) for CTRL run **(a)**, NOSOA run **(b)**, and their differences **(c)**. The fields are extracted along the cross section A (see Fig. 12) at 06:00 UTC of 17 May. The x axis reports the west–east distance in kilometres along the cross section.

by long-range transport of Saharan dust with the passage of southerly fronts (23–31 May).

The model reproduces the variations of meteorological variables as a function of the synoptic frame. The model broadly captures the inter- and infra-diurnal variability of O_3 and NO_x at the surface. The concentration of NH_3 is underestimated. Concentrations of HNO_3 and HONO are reproduced with poor correlation. Simulated SO_2 shows a positive bias of +90 %, probably due to overestimated point sources. Surface aerosol mass of SO_4, NO_3, NH_4, and OM is simulated with a correlation larger than 0.55. Their diurnal variations as a function of the synoptic frame are resolved by the model. The bias of simulated inorganic aerosol mass is explainable together with error of SO_2, NH_3, and HNO_3 in terms of anthropogenic emissions and the approximation to instantaneous thermodynamic equilibrium. The performances in reproducing the surface aerosol mass found here are comparable to other European studies where these variables are simulated with correlations range from 0.5 to 0.7 (e.g., Lecœur and Signeur, 2013; Zhang et al., 2013b; Balzarini et al., 2015, for inorganic species; Athanasopoulou et al., 2013; Fountoukis et al., 2014; Li et al., 2013; Knote et al., 2011; for organic aerosols).

The analysis of aircraft data reveals that WRF-Chem captures the aerosol mass trend both in the PBL and the free troposphere (FT). The predicted aloft aerosol mass of each species is within the observed values range, but the model does not capture the full range of the measured concentrations; the modelled standard deviations of aerosol mass are lower than those observed. Nevertheless, SO_4 (NO_3 and NH_4) mass is overpredicted (underpredicted) in more than half of the flights. SO_4 bias is attributable to the SO_2 excess and to a potential overproduction within the cloud chemistry scheme. The negative bias of NO_3 and NH_4 could be explained by a low concentration of NH_3 that limits the formation of the ammonium–nitrate. The simulated OM concentration is at lower end of the observed mass. The bias is attributable to the missing aqueous chemistry processes of organic compounds, uncertainties in meteorological fields, to assumptions on the VBS approach such as the SOA formation pathways, oxidation rate, and dry deposition velocity of organic condensable vapours. Another source of error in simulating SOA are the uncertainties in the anthropogenic emissions of primary organic carbon and in the factor (1.6) used to convert them to POM. In general, the statistical analysis reveals that the predicted average concentrations of inorganic aerosols show absolute error of 2–8 % in the PBL, while the NO_3 and NH_4 are simulated with a bias of +14 and +20 % (+0.3 and +0.2 $\mu g\,m^{-3}$), respectively, in the FT. The mean OM mass is underestimated by a factor of 2 and 3

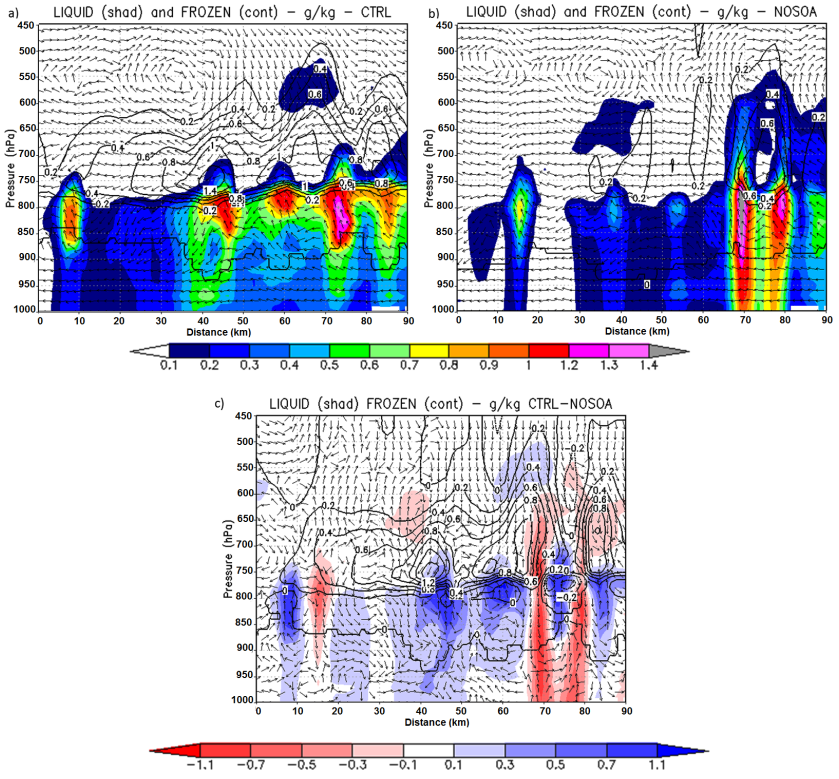

Figure 17. As in Fig. 16, but for water (colour), and frozen (black contours) hydrometeors.

in the PBL and FT, respectively. These biases are similar to those reported by Fast et al. (2014) comparing WRF-Chem (but with a different chemistry package) to aircraft data performed over California. Indeed, they found an absolute mean bias of about 0.01–0.2, 0.03–0.6, 0.1–0.45, 0.2–0.57 $\mu g\,m^{-3}$ for SO_4, NO_3, NH_4, and OM, respectively. However, we highlighted that the comparison of aerosol composition predicted by the model with AMS measurements could be affected by a bias because the model concentrations are representative of $PM_{2.5}$ particles and AMS collects aerosols with a diameter only between 100 and 700 nm.

Condensation nuclei (CN) are overestimated by a factor of 1.4 and 1.7 in the PBL and FT, respectively. However, in some cases, the predicted CN are overestimated by a factor of 3. Predicted CN show higher variability than measurements. The model correlation with observed CN is 0.40 and 0.74 in PBL and FT, respectively. These values are consistent with the 0.61 below 10 km of altitude found by Luo and Yu (2011) in the eastern USA with WRF-Chem including an advanced aerosol microphysical model. Model biases in predicting CN are attributable in large part to the uncertainties of primary particle emissions (mostly in the PBL) and to the nucleation rate.

The bias of simulated CCN is more contained with respect to that of CN. The CCN efficiency (CCN / CN ratio) is underestimated by a factor of 1.5 and 3.8 in the PBL and FT, respectively. This could be due to a low number of particles in the accumulation and coarse mode or to uncertainties in the hygroscopicity of aerosol particles. CCN / CN ratio represents the ability of aerosol particles to nucleate in cloud droplets. Therefore, its misrepresentation may lead to issues in the simulation of cloud droplet number. In other words, the uncertainties in CCN efficiency is a general modelling problem that may prevent a correct representation of the amplitude of the aerosol–cloud interaction, i.e. the response of microphysical cloud properties to the variation of CCN concentrations. This issue surely deserves and warrants further insight in the future; studies on the sensitive of the CCNs to emission distribution in the log-normal modes, aerosol hygroscopicity, and updraft velocity are desirable to improve the aerosol activation in the models.

The bias of simulated CN affects the prediction of droplet R_e, aerosol optical thickness (AOT), cloud water path (CWP), and cloud optical thickness (COT). The comparison with MODIS data shows that the model overestimates the AOT. The AOT averaged over the entire domain on a single day are 0.38 ± 0.12 and 0.42 ± 0.10 for MODIS and WRF-Chem data, respectively. The domain-averaged R_e of liquid cloud droplets is underestimated by a factor of 1.5 in all the periods examined in the main text. Modelled mean cloud liquid water path (LWP) is also overestimated by a factor of 1.1–1.6. The consequence of the negative (positive) bias of R_e (LWP) is the overestimation of average liquid COT by a few percent up to 42 %. CWP and COT of all cloud phases

are systematically in 2 out of 3 periods analysed. Predicted domain average of CWP presents a bias that ranges from 41 to 80 %, whereas the bias of COT is about 15 % in P1 and P3. The overprediction of CWP could be due to the overestimation of droplet number concentration that results from the overestimation of CN, and to inefficient autoconversion of cloud water to rain. The reader should note that the model errors found here are different from the study conducted with WRF-Chem by Yang et al. (2011) on the modelling of marine stratocumulus in the south-east Pacific, where SOA formation was not included in the simulations. Those authors reported a bias of +30 % in reproducing the COT, while CWP was underestimated by a factor of 1.3.

In summary, the model behaviour of this new chemistry option in WRF-Chem in simulating the relationship between aerosol and cloud fields may be summarized in this way. The overestimation of CN results in the overprediction of the CCN. A higher number of CCN leads to clouds with a higher number of cloud droplets, higher water content, smaller droplets, and clouds optically deeper.

As test application of the new chemistry option, we performed a sensitivity simulation where SOA mass concentration is set to zero. The aim was to answer two questions:

1. Does the introduction of SOA particles improve the numerical prediction of cloud fields?

   The introduction of SOA in the numerical simulations improves the predicted spatial pattern of microphysical and optical properties of cloud in liquid and all phases. NOSOA runs show an average R_e larger than CTRL. The analysis of LWP distribution function does not reveal a clear difference between CTRL and NOSOA simulations during the examined periods, only the domain averages allow one to establish that LWP values predicted by the CTRL run are closer to the observed means than NOSOA. Conversely, including SOA in the numerical prediction improves the distribution function of liquid COT with respect to NOSOA in two out of three cases. In these two cases, NOSOA has up to 10 % more optically thin liquid clouds (COT < 40) with respect to CTRL. Finally, with regards to CWP and COT (all phase), including SOA aerosol particles in the runs, the WRF-Chem improves to reproduce the observed pattern of observed CWP and COT.

2. What is the impact of SOA particles on cloud development?

   The analysis was conducted on a convective system. The simulated radar reflectivity is larger for run with SOA; i.e. the intensity of the storm is stronger in the CTRL run. The CTRL simulation exhibits a larger number of hydrometeors and stronger updrafts and downdrafts. The larger differences in the simulated fields of vertical wind and hydrometeors are associated with the larger differences of $PM_{2.5}$ mass located at the cloud base.

On the basis of the results discussed in this work, the option RACM-MADE-VBS coupled with cloud microphysics and radiation allows the WRF-Chem community to use a powerful tool for the study of the aerosol–cloud interactions, improved in terms of representation of the aerosol processes with respect to previous versions based on the RADM/MADE/SORGAM scheme.

For the future, there is still large space for improvements. For example, a more advanced treatment of deposition of organic condensable vapours is desirable. Moreover, the missing production of SOA in cloud is a gap that should also be filled. Finally, the extension of aerosol–cloud interaction to the ice-phase would lead to a complete representation of the aerosol indirect effects.

Appendix A: Technical details of coupling of VBS scheme with radiation and microphysics schemes

The new chemistry option in namelist.input is *chem_opt=44*. It works with both Lin and Morrison microphysics scheme, Goddard and RRTM shortwave scheme, and RRTM longwave parameterization. The coupling of a new scheme for SOA production with microphysics and radiative processes requires several modifications to code:

1. The first step is to create a new chemistry option. The package racm_soa_vbs_aqchem_kpp (chemopt==44) has been added to /Registry/registry.chem together with some new model variables for the cloud-borne organic aerosols called, for example, *asoa1cwi*, *asoa1cwj*, etc.

2. New chemistry package is a KPP option. Therefore, we created a new subdirectory in */chem/KPP/mechanisms/racm_soa_vbs_aqchem* containing the files (*.spc, *.eqn, *.kpp, and *.def) which defined the chemical model species and constants, chemical reactions in KPP format, model description, computer language, precision, and integrator. The files are the same as those used in *racm_soa_vbs_kpp* package (chemopt==108).

3. The last step is to update the subroutines in the *chem* subdirectory. In order to call necessary subroutines, the modules that we modified are

   - *chemics_init.F*
   - *module_input_chem_data.F*
   - *mechanism_driver.F*
   - *cloudchem_driver.F*
   - *module_sorgam_aqchem.F*
   - *module_wetscav_driver.F*
   - *module_aerosols_soa_vbs.F*
   - *aerosol_driver.F*
   - *dry_dep_driver.F*
   - *module_mixactivate_wrappers.F*
   - *emissions_driver.F*
   - *module_bioemi_megan2.F*
   - *optical_driver.F*
   - *module_optical_averaging.F*
   - *module_ctrans_grell.F*

Appendix B: Statistical indices used in the model evaluation

Let Obs_i and Mod_i be the observed and modelled values at time i, and N the number of observations.

- The Pearson's correlation (r):

$$r = \frac{1}{N}\sum_{i=1}^{N} Z_i(\mathrm{Mod}) \cdot Z_i(\mathrm{Obs})$$
$$Z(X) = \frac{X - \langle X \rangle}{\sigma_X},$$

  where X is a generic vector, $Z(X)$ is its standard score, and σ_X is the standard deviation.

- Mean bias:

$$\mathrm{MB} = \frac{1}{N}\left(\sum_{i=1}^{N} \mathrm{Mod}_i - \mathrm{Obs}_i\right),$$

- Normalized mean bias (NMB):

$$\mathrm{NMB} = \frac{1}{N}\sum_{i=1}^{N} \frac{\mathrm{Mod}_i - \mathrm{Obs}_i}{\mathrm{Obs}_i} \times 100,$$

- Normalized mean gross error (NMGE):

$$\mathrm{NMGE} = \frac{1}{N}\sum_{i=1}^{N} \frac{|\mathrm{Mod}_i - \mathrm{Obs}_i|}{\mathrm{Obs}_i} \times 100.$$

Code availability

The code updated, described, and evaluated here will be incorporated in the next available release of WRF-Chem. The users will be able to freely download the code from the WRF website (http://www2.mmm.ucar.edu/wrf/users/download/get_source.html). A general WRF-Chem user's guide is also available online (http://ruc.noaa.gov/wrf/WG11/).

The Supplement related to this article is available online at doi:10.5194/gmd-8-2749-2015-supplement.

Acknowledgements. This work was founded by the University of L'Aquila (Italy) and Regione Abruzzo in the frame of the "High Formation Project" (P.O.F.S.E 2007-2013), and the Italian Space Agency in the frame of the PRIMES (contract I/017/11/0) project. Paolo Tuccella is grateful to the National and Oceanic Administration (NOAA) of Boulder (CO, USA) for the hospitality, to Ravan Ahmadov and Stuart McKeen for the precious and profitable discussions about the parameterization for secondary organic aerosol, and to Steven Peckham for the assistance in the implementation of the new chemical option in the repository version of WRF-Chem. We are grateful to the Euro-Mediterranean Center on Climate Change (CMCC) for having made available their supercomputer to perform the numerical simulations. The authors thank Hugo Denier van der Gon for providing the TNO emissions. Finally, the authors are grateful to two anonymous reviewers for their suggestions that helped to improve this paper.

Edited by: F. O'Connor

References

Aan de Brugh, J. M. J., Henzing, J. S., Schaap, M., Morgan, W. T., van Heerwaarden, C. C., Weijers, E. P., Coe, H., and Krol, M. C.: Modelling the partitioning of ammonium nitrate in the convective boundary layer, Atmos. Chem. Phys., 12, 3005–3023, doi:10.5194/acp-12-3005-2012, 2012.

Abdul-Razzak, H. and Ghan, S. J.: A parameterization of aerosol activation, 2, Multiple aerosol types, J. Geophys. Res., 105, 6837–6844, doi:10.1029/1999JD901161, 2000.

Abdul-Razzak, H. and Ghan, S. J.: A Parameterization of Aerosol Activation. 3. Sectional Representation, J. Geophys. Res., 107, 4026, doi:10.1029/2001JD000483, 2002.

Ackermann, I. J., Hass, H., Memmsheimer, M., Ebel, A., Binkowski, F. S., and Shankar, U.: Modal aerosol dynamics model for Europe: development and first applications, Atmos. Environ., 32, 2981–2999, doi:10.1016/S1352-2310(98)00006-5, 1998.

Ahmadov, R., McKeen, S. A., Robinson, A., Bahreini, R., Middlebrook, A., de Gouw, J., Meagher, J., Hsie, E., Edgerton, E., Shaw, S., and Trainer, M.: A volatility basis set model for summertime secondary organic aerosols over the eastern United States in 2006, J. Geophys. Res., 117, D06301, doi:10.1029/2011JD016831, 2012.

Andreae, M. O. and Rosenfeld, D.: Aerosol-cloud-precipitation interactions. Part 1. The nature and sources of cloud-active aerosols, Earth-Sci. Rev., 89, 13–41, doi:10.1016/j.earscirev.2008.03.001, 2008.

Asmi, E., Freney, E., Hervo, M., Picard, D., Rose, C., Colomb, A., and Sellegri, K.: Aerosol cloud activation in summer and winter at puy-de-Dôme high altitude site in France, Atmos. Chem. Phys., 12, 11589–11607, doi:10.5194/acp-12-11589-2012, 2012.

Athanasopoulou, E., Vogel, H., Vogel, B., Tsimpidi, A. P., Pandis, S. N., Knote, C., and Fountoukis, C.: Modeling the meteorological and chemical effects of secondary organic aerosols during an EUCAARI campaign, Atmos. Chem. Phys., 13, 625–645, doi:10.5194/acp-13-625-2013, 2013.

Baklanov, A., Schlünzen, K., Suppan, P., Baldasano, J., Brunner, D., Aksoyoglu, S., Carmichael, G., Douros, J., Flemming, J., Forkel, R., Galmarini, S., Gauss, M., Grell, G., Hirtl, M., Joffre, S., Jorba, O., Kaas, E., Kaasik, M., Kallos, G., Kong, X., Korsholm, U., Kurganskiy, A., Kushta, J., Lohmann, U., Mahura, A., Manders-Groot, A., Maurizi, A., Moussiopoulos, N., Rao, S. T., Savage, N., Seigneur, C., Sokhi, R. S., Solazzo, E., Solomos, S., Sørensen, B., Tsegas, G., Vignati, E., Vogel, B., and Zhang, Y.: Online coupled regional meteorology chemistry models in Europe: current status and prospects, Atmos. Chem. Phys., 14, 317–398, doi:10.5194/acp-14-317-2014, 2014.

Balzarini, A., Pirovano, G., Honzak, L., Zabkar, R., Curci, G., Forkel, R., Hirtl, M., San José, R., Tuccella, P., and Grell, G. A.: WRF-Chem model sensitivity to chemical mechanism choice in reconstructing aerosol optical properties, Atmos. Environ., 115, 604–619, doi:10.1016/j.atmosenv.2014.12.033, 2015.

Barnard, J. C., Fast, J. D., Paredes-Miranda, G., Arnott, W. P., and Laskin, A.: Technical Note: Evaluation of the WRF-Chem "Aerosol Chemical to Aerosol Optical Properties" Module using data from the MILAGRO campaign, Atmos. Chem. Phys., 10, 7325–7340, doi:10.5194/acp-10-7325-2010, 2010.

Bao, J.-W., Michelson, S. A., McKeen, S. A., and Grell, G. A.: Meteorological evaluation of a weather-chemistry forecasting model using observations from the TEXAS AQS 2000 field experiment, J. Geophys. Res., 110, D21105, doi:10.1029/2004JD005024, 2005.

Bègue, N., Tulet, P., Pelon, J., Aouizerats, B., Berger, A., and Schwarzenboeck, A.: Aerosol processing and CCN formation of an intense Saharan dust plume during the EUCAARI 2008 campaign, Atmos. Chem. Phys., 15, 3497–3516, doi:10.5194/acp-15-3497-2015, 2015.

Bei, N., Li, G., and Molina, L. T.: Uncertainties in SOA simulations due to meteorological uncertainties in Mexico City during MILAGRO-2006 field campaign, Atmos. Chem. Phys., 12, 11295–11308, doi:10.5194/acp-12-11295-2012, 2012.

Bessagnet, B., Seigneur, C., and Menut, L.: Impact of dry deposition of semi-volatile organic compounds on secondary organic aerosols, Atmos. Environ., 44, 1781–1787, doi:10.1016/j.atmosenv.2010.01.027, 2010.

Boucher, O., Randall, D., Artaxo, P., Bretherton, C., Feingold, G., Forster, P., Kerminen, V.-M., Kondo, Y., Liao, H., Lohmann, U., Rasch, P., Satheesh, S. K., Sherwood, S., Stevens B., and Zhang, X. Y.: Clouds and Aerosols, in: Climate Change 2013: The Physical Science Basis. Contribution of Working Group I to the Fifth Assessment Report of the Intergovernmental Panel on Climate Change, edited by: Stocker, T. F., Qin, D., Plattner, G.-K., Tig-

nor, M., Allen, S. K., Boschung, J., Nauels, A., Xia, Y., Bex, V., and Midgley, P. M., Cambridge University Press, Cambridge, United Kingdom and New York, NY, USA,2013.

Brunner, D., Jorba, O., Savage, N., Eder, B., Makar, P., Giordano, L., Badia, A., Balzarini, A., Baro, R., Bianconi, R., Chemel, C., Forkel, R., Jimenez-Guerrero, P., Hirtl, M., Hodzic, A., Honzak, L., Im, U., Knote, C., Kuenen, J. P. P., Makar, P. A., Manders-Groot, A., Neal, L., Perez, J. L., Pirovano, G., San Jose, R., Savage, N., Schroder, W., Sokhi, R. S., Syrakov, D., Torian, A., Tuccella, P., Werhahn, K., Wolke, R., van Meijgaard, E., Yahya, K., Zabkar, R., Zhang, Y., Zhang, J., Hogrefe, C., and Galmarini, S.: Evaluation of the meteorological performance of coupled chemistry-meteorology models in phase 2 of the air quality model evaluation international initiative, Atmos. Environ., 115, 470–498, doi:10.1016/j.atmosenv.2014.12.032, 2015.

Chapman, E. G., Gustafson Jr., W. I., Easter, R. C., Barnard, J. C., Ghan, S. J., Pekour, M. S., and Fast, J. D.: Coupling aerosol-cloud-radiative processes in the WRF-Chem model: Investigating the radiative impact of elevated point sources, Atmos. Chem. Phys., 9, 945–964, doi:10.5194/acp-9-945-2009, 2009.

Clarke, A. and Kapustin, A.: Hemispheric Aerosol Vertical Profiles: Anthropogenic Impacts on Optical Depth and Cloud Nuclei, Science, 329, 1488, doi:10.1126/science.1188838, 2010.

Christensen, M. W. and Stephens, G. L.: Microphysical and macrophysical responses of marine stratocumulus polluted by underlying ships: Evidence of cloud deepening, J. Geophys. Res., 116, D03201, doi:10.1029/2010JD014638, 2011.

Crumeyrolle, S., Schwarzenboeck, A., Roger, J. C., Sellegri, K., Burkhart, J. F., Stohl, A., Gomes, L., Quennehen, B., Roberts, G., Weigel, R., Villani, P., Pichon, J. M., Bourrianne, T., and Laj, P.: Overview of aerosol properties associated with air masses sampled by the ATR-42 during the EUCAARI campaign (2008), Atmos. Chem. Phys., 13, 4877–4893, doi:10.5194/acp-13-4877-2013, 2013.

Curci, G., Ferrero, L., Tuccella, P., Barnaba, F., Angelini, F., Bolzacchini, E., Carbone, C., Denier van der Gon, H. A. C., Facchini, M. C., Gobbi, G. P., Kuenen, J. P. P., Landi, T. C., Perrino, C., Perrone, M. G., Sangiorgi, G., and Stocchi, P.: How much is particulate matter near the ground influenced by upper-level processes within and above the PBL? A summertime case study in Milan (Italy) evidences the distinctive role of nitrate, Atmos. Chem. Phys., 15, 2629–2649, doi:10.5194/acp-15-2629-2015, 2015a.

Curci, G., Hogrefe, C., Bianconi, R., Im, U., Balzarini, A., Baro, R., Brunner, D., Forkel, R., Giordano, L., Hirtl, M., Honzak, L., Jimenez-Guerrero, P., Knote, C., Langer, M., Makar, P.A., Pirovano, G., Perez, J.L., San Jose, R., Syrakov, D., Tuccella, P., Werhahn, J., Wolke, R., Zabkar, R., Zhang, J., Galmarini, S.: Uncertainties of simulated aerosol optical properties induced by assumptions on aerosol physical and chemical properties: an AQMEII-2 perspective, Atmos. Environ., 115, 541–552, doi:10.1016/j.atmosenv.2014.09.009, 2015b.

Easter, R. C., Ghan, S. J., Zhang, Y., Saylor, R. D., Chapman, E. G., Laulainen, N. S., Abdul-Razzak, H., Leung, L. R., Bian, X., and Zaveri, R. A.: MIRAGE: Model Description and Evaluation of Aerosols and Trace Gases, J. Geophys. Res., 109, D20210, doi:10.1029/2004JD004571, 2004.

Ebert, E. E. and Curry, J. A.: A parameterization of ice cloud optical properties for climate models, J. Geophys. Res., 97, 3831–3836, doi:10.1029/91JD02472, 1992.

Elleman, R. A. and Covert, D. S.: Aerosol size distribution modeling with the Community Multiscale Air Quality modeling system in the Pacific Northwest: 3. Size distribution of particles emitted into a mesoscale model, J. Geophys. Res., 115, D03204, doi:10.1029/2009JD012401, 2010.

Emmons, L. K., Walters, S., Hess, P. G., Lamarque, J.-F., Pfister, G. G., Fillmore, D., Granier, C., Guenther, A., Kinnison, D., Laepple, T., Orlando, J., Tie, X., Tyndall, G., Wiedinmyer, C., Baughcum, S. L., and Kloster, S.: Description and evaluation of the Model for Ozone and Related chemical Tracers, version 4 (MOZART-4), Geosci. Model Dev., 3, 43–67, doi:10.5194/gmd-3-43-2010, 2010.

Ervens, B., Turpin, B. J., and Weber, R. J.: Secondary organic aerosol formation in cloud droplets and aqueous particles (aqSOA): a review of laboratory, field and model studies, Atmos. Chem. Phys., 11, 11069–11102, doi:10.5194/acp-11-11069-2011, 2011.

Fast, J. D., Gustafson Jr., W. I., Easter, R. C., Zaveri, R. A., Barnard, J. C., Chapman, E. G., Grell, G. A., and Peckham, S. E.: Evolution of ozone, particulate, and aerosol direct radiative forcing in the vicinity of Houston using a fully coupled meteorology-chemistryaerosol model, J. Geophys. Res., 111, D21305, doi:10.1029/2005JD006721, 2006.

Fast, J. D., Allan, J., Bahreini, R., Craven, J., Emmons, L., Ferrare, R., Hayes, P. L., Hodzic, A., Holloway, J., Hostetler, C., Jimenez, J. L., Jonsson, H., Liu, S., Liu, Y., Metcalf, A., Middlebrook, A., Nowak, J., Pekour, M., Perring, A., Russell, L., Sedlacek, A., Seinfeld, J., Setyan, A., Shilling, J., Shrivastava, M., Springston, S., Song, C., Subramanian, R., Taylor, J. W., Vinoj, V., Yang, Q., Zaveri, R. A., and Zhang, Q.: Modeling regional aerosol and aerosol precursor variability over California and its sensitivity to emissions and long-range transport during the 2010 CalNex and CARES campaigns, Atmos. Chem. Phys., 14, 10013–10060, doi:10.5194/acp-14-10013-2014, 2014.

Fountoukis, C., Megaritis, A. G., Skyllakou, K., Charalampidis, P. E., Pilinis, C., Denier van der Gon, H. A. C., Crippa, M., Canonaco, F., Mohr, C., Prévôt, A. S. H., Allan, J. D., Poulain, L., Petäjä, T., Tiitta, P., Carbone, S., Kiendler-Scharr, A., Nemitz, E., O'Dowd, C., Swietlicki, E., and Pandis, S. N.: Organic aerosol concentration and composition over Europe: insights from comparison of regional model predictions with aerosol mass spectrometer factor analysis, Atmos. Chem. Phys., 14, 9061–9076, doi:10.5194/acp-14-9061-2014, 2014.

Ghan, S. J., Leung, L. R., Easter, R. C., and Abdul-Razzak, H.: Pre-diction of Droplet Number in a General Circulation Model, J. Geophys. Res., 102, 21777–21794, doi:10.1029/97JD01810, 1997.

Grell, G. A., Peckham, S. E., McKeen, S., Schmitz, R., Frost, G., Skamarock, W. C., and Eder, B.: Fully coupled "online" chemistry within the WRF model, Atmos. Environ., 39, 6957–6975, doi:10.1016/j.atmosenv.2005.04.027, 2005.

Guenther, A., Karl, T., Harley, P., Wiedinmyer, C., Palmer, P. I., and Geron, C.: Estimates of global terrestrial isoprene emissions using MEGAN (Model of Emissions of Gases and Aerosols from Nature), Atmos. Chem. Phys., 6, 3181–3210, doi:10.5194/acp-6-3181-2006, 2006.

Hallquist, M., Wenger, J. C., Baltensperger, U., Rudich, Y., Simpson, D., Claeys, M., Dommen, J., Donahue, N. M., George, C., Goldstein, A. H., Hamilton, J. F., Herrmann, H., Hoffmann, T., Iinuma, Y., Jang, M., Jenkin, M. E., Jimenez, J. L., Kiendler-Scharr, A., Maenhaut, W., McFiggans, G., Mentel, Th. F., Monod, A., Prévôt, A. S. H., Seinfeld, J. H., Surratt, J. D., Szmigielski, R., and Wildt, J.: The formation, properties and impact of secondary organic aerosol: current and emerging issues, Atmos. Chem. Phys., 9, 5155–5236, doi:10.5194/acp-9-5155-2009, 2009.

Haywood J. and Boucher O.: Estimates of the direct and indirect aerosol radiative forcing due to tropospheric aerosols: a review, Rev. Geophys., 38, 513–543, doi:10.1029/1999RG000078, 2000.

Hamburger, T., McMeeking, G., Minikin, A., Birmili, W., Dall'Osto, M., O'Dowd, C., Flentje, H., Henzing, B., Junninen, H., Kristensson, A., de Leeuw, G., Stohl, A., Burkhart, J. F., Coe, H., Krejci, R., and Petzold, A.: Overview of the synoptic and pollution situation over Europe during the EUCAARI-LONGREX field campaign, Atmos. Chem. Phys., 11, 1065–1082, doi:10.5194/acp-11-1065-2011, 2011.

Hansen, J., Sato, M., and Ruedy, R.: Radiative forcing and climate response, J. Geophys. Res., 102, 6831–6894, doi:10.1029/96JD03436, 1997.

Henrich, F., Siebert, H., Jakel, E., Shaw, R. A., and Wendisch, M.: Collocated measurements of boundary layer cloud microphysical and radiative properties: a feasibility study, J. Geophys. Res., 115, D24214, doi:10.1029/2010JD013930, 2010.

Holt, T. R., Niyogi, D., Chen, F., Manning, K., LeMone, M. A., and Qureshi, A.: Effect of Land–Atmosphere Interactions on the IHOP 24–25 May 2002 Convection Case, Mon. Weather Rev., 134, 113–133, doi:10.1175/MWR3057.1, 2006.

Im, U., Bianconi, R., Solazzo, E., Kioutsioukis, I., Badia, A., Balzarini, A., Baro, R., Bellasio, R., Brunner, D., Chemel, C., Curci, G., Denier van der Gon, H., Flemming, J., Forkel, R., Giordano, L., Jimenez-Guerrero, P., Hirtl, M., Hodzic, A., Honzak, L., Jorba, O., Knote, C., Makar, P. A., Manders-Groot, A., Neal, L., Perez, J. L., Pirovano, G., Pouliot, G., San Jose, R., Savage, N., Schroder, W., Sokhi, R. S., Syrakov, D., Torian, A., Tuccella, P., Wang, K., Werhahn, J., Wolke, R., Zabkar, R., Zhang, Y., Zhang, J., Hogrefe, C., and Galmarini, S.: Evaluation of operational online-coupled regional air quality models over Europe and North America in the context of AQMEII phase 2. Part II: Particulate Matter, Atmos. Environ., 115, 421–441, doi:10.1016/j.atmosenv.2014.08.072, 2015.

King, N. J., Bower, K. N., Crosier, J., and Crawford, I.: Evaluating MODIS cloud retrievals with in situ observations from VOCALS-REx, Atmos. Chem. Phys., 13, 191–209, doi:10.5194/acp-13-191-2013, 2013.

Knote, C., Brunner, D., Vogel, H., Allan, J., Asmi, A., Äijälä, M., Carbone, S., van der Gon, H. D., Jimenez, J. L., Kiendler-Scharr, A., Mohr, C., Poulain, L., Prévôt, A. S. H., Swietlicki, E., and Vogel, B.: Towards an online-coupled chemistry-climate model: evaluation of trace gases and aerosols in COSMO-ART, Geosci. Model Dev., 4, 1077–1102, doi:10.5194/gmd-4-1077-2011, 2011.

Knote, C., Tuccella, P., Curci, G., Emmons, L., Orlando, J. J., Madronich, S., Barò, R., Jimìenez-Guerrero, P., Luecken, D., Hogrefe, C., Forkel, R., Werhahn, J., Hirtl, M., Pìrez, J. L., San Josée, R., Giordano, L., Brunner, D., Yahya, K., and Zhang, Y.: Influence of the choice of gas-phase mechanism on predictions of key gaseous pollutants during the AQMEII phase-2 intercomparison, Atmos. Environ., 115, 553–568, doi:10.1016/j.atmosenv.2014.11.066, 2015a.

Knote, C., Hodzic, A., and Jimenez, J. L.: The effect of dry and wet deposition of condensable vapors on secondary organic aerosols concentrations over the continental US, Atmos. Chem. Phys., 15, 1–18, doi:10.5194/acp-15-1-2015, 2015b.

Koren, I., Altaratz, O., Remer, L. A., Feingold, G., Martins, J. V., and Heiblum, R. H.: Aerosol-induced intensification of rain from the tropics to the mid-latitudes, Nat. Geosci., 5, 118–122, doi:10.1038/ngeo1364, 2012.

Kuenen, J. J. P., Visschedijk, A. J. H., Jozwicka, M., and Denier van der Gon, H. A. C.: TNO-MACC_II emission inventory; a multi-year (2003–2009) consistent high-resolution European emission inventory for air quality modelling, Atmos. Chem. Phys., 14, 10963–10976, doi:10.5194/acp-14-10963-2014, 2014.

Kulmala, M., Asmi, A., Lappalainen, H. K., Baltensperger, U., Brenguier, J.-L., Facchini, M. C., Hansson, H.-C., Hov, Ø., O'Dowd, C. D., Pöschl, U., Wiedensohler, A., Boers, R., Boucher, O., de Leeuw, G., Denier van der Gon, H. A. C., Feichter, J., Krejci, R., Laj, P., Lihavainen, H., Lohmann, U., McFiggans, G., Mentel, T., Pilinis, C., Riipinen, I., Schulz, M., Stohl, A., Swietlicki, E., Vignati, E., Alves, C., Amann, M., Ammann, M., Arabas, S., Artaxo, P., Baars, H., Beddows, D. C. S., Bergström, R., Beukes, J. P., Bilde, M., Burkhart, J. F., Canonaco, F., Clegg, S. L., Coe, H., Crumeyrolle, S., D'Anna, B., Decesari, S., Gilardoni, S., Fischer, M., Fjaeraa, A. M., Fountoukis, C., George, C., Gomes, L., Halloran, P., Hamburger, T., Harrison, R. M., Herrmann, H., Hoffmann, T., Hoose, C., Hu, M., Hyvärinen, A., Hõrrak, U., Iinuma, Y., Iversen, T., Josipovic, M., Kanakidou, M., Kiendler-Scharr, A., Kirkevåg, A., Kiss, G., Klimont, Z., Kolmonen, P., Komppula, M., Kristjánsson, J.-E., Laakso, L., Laaksonen, A., Labonnote, L., Lanz, V. A., Lehtinen, K. E. J., Rizzo, L. V., Makkonen, R., Manninen, H. E., McMeeking, G., Merikanto, J., Minikin, A., Mirme, S., Morgan, W. T., Nemitz, E., O'Donnell, D., Panwar, T. S., Pawlowska, H., Petzold, A., Pienaar, J. J., Pio, C., Plass-Duelmer, C., Prévôt, A. S. H., Pryor, S., Reddington, C. L., Roberts, G., Rosenfeld, D., Schwarz, J., Seland, Ø., Sellegri, K., Shen, X. J., Shiraiwa, M., Siebert, H., Sierau, B., Simpson, D., Sun, J. Y., Topping, D., Tunved, P., Vaattovaara, P., Vakkari, V., Veefkind, J. P., Visschedijk, A., Vuollekoski, H., Vuolo, R., Wehner, B., Wildt, J., Woodward, S., Worsnop, D. R., van Zadelhoff, G.-J., Zardini, A. A., Zhang, K., van Zyl, P. G., Kerminen, V.-M., S Carslaw, K., and Pandis, S. N.: General overview: European Integrated project on Aerosol Cloud Climate and Air Quality interactions (EUCAARI) – integrating aerosol research from nano to global scales, Atmos. Chem. Phys., 11, 13061–13143, doi:10.5194/acp-11-13061-2011, 2011.

Lecœur, È. and Seigneur, C.: Dynamic evaluation of a multi-year model simulation of particulate matter concentrations over Europe, Atmos. Chem. Phys., 13, 4319–4337, doi:10.5194/acp-13-4319-2013, 2013.

Lee, L. A., Pringle, K. J., Reddington, C. L., Mann, G. W., Stier, P., Spracklen, D. V., Pierce, J. R., and Carslaw, K. S.: The magnitude and causes of uncertainty in global model simulations of cloud condensation nuclei, Atmos. Chem. Phys., 13, 8879–8914, doi:10.5194/acp-13-8879-2013, 2013.

Li, X., Rohrer, F., Hofzumahaus, A., Brauers, T., Häseler, R., Bohn, B., Broch, S., Fuchs, H., Gomm, S., Holland, F., Jäger, J., Kaiser, J., Keutsch, F. N., Lohse, I., Lu, K., Tillmann, R., Wegener, R., Wolfe, G. M., Mentel, F. M., Kiendler-Scharr, A., and Wahner, A.: Missing Gas-Phase Source of HONO Inferred from Zeppelin Measurements in the Troposphere, Science, 344, 292–296, doi:10.1126/science.1248999, 2014.

Li, Y. P., Elbern, H., Lu, K. D., Friese, E., Kiendler-Scharr, A., Mentel, Th. F., Wang, X. S., Wahner, A., and Zhang, Y. H.: Updated aerosol module and its application to simulate secondary organic aerosols during IMPACT campaign May 2008, Atmos. Chem. Phys., 13, 6289–6304, doi:10.5194/acp-13-6289-2013, 2013.

Li, Z., Niu, F., Fan, J., Liu, Y., Rosenfeld, D., and Ding, D.: Long-term impacts of aerosols on the vertical development of clouds and precipitation, Nat. Geosci., 4, 888–894, doi:10.1038/ngeo1313, 2011.

Lohmann, U. and Feichter, J.: Global indirect aerosol effects: a review, Atmos. Chem. Phys., 5, 715–737, doi:10.5194/acp-5-715-2005, 2005.

Luo, G. and Yu, F.: Simulation of particle formation and number concentration over the Eastern United States with the WRF-Chem + APM model, Atmos. Chem. Phys., 11, 11521–11533, doi:10.5194/acp-11-11521-2011, 2011.

Meng, Z., Dabdud, D., and Seinfeld, J. H.: Chemical coupling between atmospheric ozone and particulate matter, Science, 277, 116–119, doi:10.1126/science.277.5322.116, 1997.

Mensah, A. A., Holzinger, R., Otjes, R., Trimborn, A., Mentel, Th. F., ten Brink, H., Henzing, B., and Kiendler-Scharr, A.: Aerosol chemical composition at Cabauw, The Netherlands as observed in two intensive periods in May 2008 and March 2009, Atmos. Chem. Phys., 12, 4723–4742, doi:10.5194/acp-12-4723-2012, 2012.

Merikanto, J., Spracklen, D. V., Mann, G. W., Pickering, S. J., and Carslaw, K. S.: Impact of nucleation on global CCN, Atmos. Chem. Phys., 9, 8601–8616, doi:10.5194/acp-9-8601-2009, 2009.

Misenis, C. and Zhang, Y.: An examination of sensitivity of WRF/Chem predictions to physical parameterizations, horizontal grid spacing, and nesting options, Atmos. Res., 97, 315–334, doi:10.1016/j.atmosres.2010.04.005, 2010.

McKeen, S., Chung, S. H., Wilczak, J., Grell, G., Djalalova, I., Peckham, S., Gong, W., Bouchet, V., Moffet, R., Tang, Y., Carmichael, G. R., Mathur, R., and Yu, S.: Evaluation of several $PM_{2.5}$ forecast models using data collected during the ICARTT/NEAQS 2004 field study, J. Geophys. Res., 112, D10S20, doi:10.1029/2006JD007608, 2007.

Ngan, F., Kim, H., Lee, P., Al-Wali, K., and Dornblaser, B.: A Study of Nocturnal Surface Wind Speed Overprediction by the WRF-ARW Model in Southeastern Texas, J. Appl. Meteor. Climatol., 52, 2638–2653, doi:10.1175/JAMC-D-13-060.1, 2013.

O'Donnell, D., Tsigaridis, K., and Feichter, J.: Estimating the direct and indirect effects of secondary organic aerosols using ECHAM5-HAM, Atmos. Chem. Phys., 11, 8635–8659, doi:10.5194/acp-11-8635-2011, 2011.

Otkin, J. A. and Greenwald, T. J.: Comparison of WRF model-simulated and MODIS-derived cloud data, Mon. Weather Rev., 136, 1957–1970, doi:10.1175/2007MWR2293.1, 2008.

Painemal, D. and Zuidema, P.: Assessment of MODIS cloud effective radius and optical thickness retrievals over the Southeast Pacific with VOCALS-REx in situ measurements, J. Geophys. Res., 116, D24206, doi:10.1029/2011JD016155, 2011.

Pielke, R. A.: Influence of the spatial distribution of vegetation and soils on the prediction of cumulus convective rainfall, Rev. Geophys., 39, 151–177, doi:10.1029/1999RG000072, 2001.

Pierce, J. R. and Adams, P. J.: Uncertainty in global CCN concentrations from uncertain aerosol nucleation and primary emission rates, Atmos. Chem. Phys., 9, 1339–1356, doi:10.5194/acp-9-1339-2009, 2009.

Roelofs, G.-J., ten Brink, H., Kiendler-Scharr, A., de Leeuw, G., Mensah, A., Minikin, A., and Otjes, R.: Evaluation of simulated aerosol properties with the aerosol-climate model ECHAM5-HAM using observations from the IMPACT field campaign, Atmos. Chem. Phys., 10, 7709–7722, doi:10.5194/acp-10-7709-2010, 2010.

Rosenfeld, D., Lohmann, U., Raga, G. B., O'Dowd, C. D., Kulmala, M., Fuzzi, S., Reissel, A., and Andreae, M. O.: Flood or Drought: How do aerosols affect precipitation?, Science, 321, 1308–1313, doi:10.1126/science.1160606, 2008.

Saide, P. E., Spak, S. N., Carmichael, G. R., Mena-Carrasco, M. A., Yang, Q., Howell, S., Leon, D. C., Snider, J. R., Bandy, A. R., Collett, J. L., Benedict, K. B., de Szoeke, S. P., Hawkins, L. N., Allen, G., Crawford, I., Crosier, J., and Springston, S. R.: Evaluating WRF-Chem aerosol indirect effects in Southeast Pacific marine stratocumulus during VOCALS-REx, Atmos. Chem. Phys., 12, 3045–3064, doi:10.5194/acp-12-3045-2012, 2012.

Schell, B., Ackermann, I. J., Hass, H., Binkowski, F. S., and Ebel, A.: Modeling the formation of secondary organic aerosol within a comprehensive air quality model system, J. Geophys. Res., 106, 28275–28293, doi:10.1029/2001JD000384, 2001.

Scott, C. E., Rap, A., Spracklen, D. V., Forster, P. M., Carslaw, K. S., Mann, G. W., Pringle, K. J., Kivekäs, N., Kulmala, M., Lihavainen, H., and Tunved, P.: The direct and indirect radiative effects of biogenic secondary organic aerosol, Atmos. Chem. Phys., 14, 447–470, doi:10.5194/acp-14-447-2014, 2014.

Sotiropoulou, R. E. P., Tagaris, E., Pilinis, C., Anttila, T., and Kulmala, M.: Modeling new particle formation during air pollution episodes: Impacts on aerosol and cloud condensation nuclei, Aerosol Sci. Technol., 40, 557–572, doi:10.1080/02786820600714346, 2006.

Spracklen, D. V., Carslaw, K. S., Kulmala, M., Kerminen, V.-M., Mann, G. W., and Sihto, S.-L.: The contribution of boundary layer nucleation events to total particle concentrations on regional and global scales, Atmos. Chem. Phys., 6, 5631–5648, doi:10.5194/acp-6-5631-2006, 2006.

Stern, R., Builtjes, P., Shaap, M., Timmermans, R., Vautard, R., Hodzic, A., Memmesheimer, M., Feldmann, H., Renner, E., Wolke, R., and Kershbaumer, A.: A model inter-comparison study focussing on episode with elevated PM_{10} concentrations, Atmos. Environ., 42, 4567–4588, doi:10.1016/j.atmosenv.2008.01.068, 2008.

Stockwell, W. R., Kirchner, F. K., Kuhn, M., and Seefeld, S.: A new mechanism for regional atmospheric chemistry modeling, J. Geophys. Res., 102, 25847–25879, doi:10.1029/97JD00849, 1997.

Ten Hoeve, J. E., Remer, L. A., and Jacobson, M. Z.: Microphysical and radiative effects of aerosols on warm clouds during the

Amazon biomass burning season as observed by MODIS: impacts of water vapor and land cover, Atmos. Chem. Phys., 11, 3021–3036, doi:10.5194/acp-11-3021-2011, 2011.

Tuccella, P., Curci, G., Visconti, G., Bessagnet, B., Menut, L., and Park, R. J.: Modeling of gas and aerosol with WRF/Chem over Europe: Evaluation and sensitivity study, J. Geophys. Res., 117, D03303, doi:10.1029/2011JD016302, 2012.

Turpin, B. J. and Lim, H.-J.: Species contributions to $PM_{2.5}$ mass concentrations: Revisiting common assumptions for estimating organic mass, Aerosol Sci. Technol., 35, 602–610, doi:10.1080/02786820152051454, 2001.

Walcek, C. J. and Taylor, G. R.: A theoretical method for computing vertical distributions of acidity and sulfate production within cumulus clouds, J. Atmos Sci., 43, 339–355, doi:10.1175/1520-0469(1986)043<0339:ATMFCV>2.0.CO;2, 1986.

Yang, Q., W. I. Gustafson Jr., Fast, J. D., Wang, H., Easter, R. C., Morrison, H., Lee, Y.-N., Chapman, E. G., Spak, S. N., and Mena-Carrasco, M. A.: Assessing regional scale predictions of aerosols, marine stratocumulus, and their interactions during VOCALS-REx using WRF-Chem, Atmos. Chem. Phys., 11, 11951–11975, doi:10.5194/acp-11-11951-2011, 2011.

Yu, S., Mathur, R., Pleim, J., Wong, D., Gilliam, R., Alapaty, K., Zhao, C., and Liu, X.: Aerosol indirect effect on the grid-scale clouds in the two-way coupled WRF-CMAQ: model description, development, evaluation and regional analysis, Atmos. Chem. Phys., 14, 11247–11285, doi:10.5194/acp-14-11247-2014, 2014.

Zhang, Y.: Online-coupled meteorology and chemistry models: history, current status, and outlook, Atmos. Chem. Phys., 8, 2895–2932, doi:10.5194/acp-8-2895-2008, 2008.

Zhang, Y., Sartelet, K., Wu, S.-Y., and Seigneur, C.: Application of WRF/Chem-MADRID and WRF/Polyphemus in Europe – Part 1: Model description, evaluation of meteorological predictions, and aerosol–meteorology interactions, Atmos. Chem. Phys., 13, 6807–6843, doi:10.5194/acp-13-6807-2013, 2013a.

Zhang, Y., Sartelet, K., Zhu, S., Wang, W., Wu, S.-Y., Zhang, X., Wang, K., Tran, P., Seigneur, C., and Wang, Z.-F.: Application of WRF/Chem-MADRID and WRF/Polyphemus in Europe – Part 2: Evaluation of chemical concentrations and sensitivity simulations, Atmos. Chem. Phys., 13, 6845-6875, doi:10.5194/acp-13-6845-2013, 2013b.

Zhao, C., Liu, X., Leung, L. R., Johnson, B., McFarlane, S. A., Gustafson Jr., W. I., Fast, J. D., and Easter, R.: The spatial distribution of mineral dust and its shortwave radiative forcing over North Africa: modeling sensitivities to dust emissions and aerosol size treatments, Atmos. Chem. Phys., 10, 8821–8838, doi:10.5194/acp-10-8821-2010, 2010.